Chapter 4

Correlation Diffusion

4.1 Introduction

In the previous two chapters I discussed the properties of diffuse photon density waves (DPDW's) and the use of these intensity waves to probe turbid media for variations in optical properties. In this chapter I show that diffusing photons can also be used to probe the dynamical properties of turbid media. Information about the dynamics is obtained from the Doppler broadening of the laser linewidth as it migrates through the medium. The broadening of the linewidth manifests itself in the intensity fluctuations of spatially coherent speckles of scattered light. On the other-hand, DPDW's manifest themselves in the average intensity of scattered light.

Although the physics for probing the dynamical properties is different, I demonstrate a theoretical model for speckle fluctuations that is completely analogous to photon diffusion. The similarity in the mathematical form of the models suggests that the observed properties of DPDW's should also be observed for speckle fluctuations.

The theoretical basis for this work dates back to the late 1960's with the development of quasi-elastic light scattering theory (QELS) for optically dilute dynamical systems which scatter light no more than once. Extensions to highly scattering systems was made in the 1980's in various guises by Bonner and Nossal [46], Pine *et al.* [48], MacKintosh and John [49], Maret and Wolf [50], and Vol'kov and Romanov [51]. The analogy of correlation transport to photon transport was first made by Ackerson

et al. [57, 58] in the 1990's in order to better understand the behavior of correlation functions in the regime between single scattering and multiple scattering.

In section 4.2 I review these theories and develop a diffusion theory for predicting speckle fluctuations. The advantage of the correlation diffusion theory over previous theories is the ease with which predictions can be made for turbid media with spatially varying dynamical and optical properties. In the final sections of this chapter, I present experimental and Monte Carlo results which demonstrate the accuracy of the correlation diffusion model for various systems. In the next chapter I present two biomedical applications for this work.

4.2   Theory

When a beam of laser light with uniform intensity is incident on a rough surface, the reflection of the beam will not have a uniform intensity but will instead be composed of many bright and dark spots. These spots are called speckles and are illustrated by fig. 4.1. The complex intensity profile arises because light is reflected in many different directions from the rough surface and thus photons that have traveled different path lengths interfere constructively and destructively at the detector. The same happens for light that has migrated through a turbid solid sample. That is, the photons exit the sample traveling in different directions and different path lengths and thus interfere constructively and destructively at the detector. If the rough surface moves or scattering particles in the turbid medium are moving, the speckle pattern will then fluctuate in time. The time scale of the intensity fluctuations depends on the motion of the surface and scattering particles.

For the turbid medium, the time scale of speckle intensity fluctuations depends on the number of interactions that detected photons have had with moving scattering particles. This section briefly reviews the theory for temporal field autocorrelation functions of light scattered from optically dilute systems such that photons scatter no more than once before being detected. I then discuss the extension of single scat-
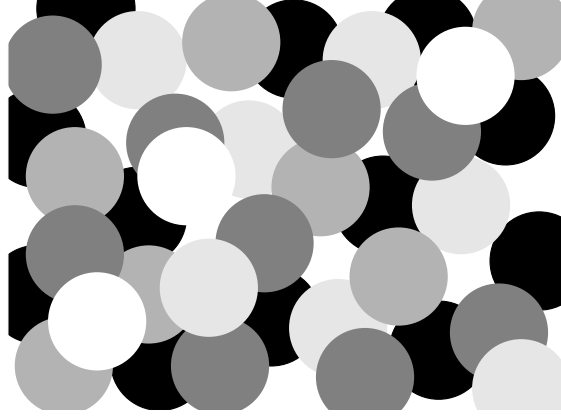
Figure 4.1: An illustration of a speckle pattern. The light regions correspond to regions of strong light intensity, and the dark regions correspond to regions of little intensity.

tering theory to systems which highly scatter light. After a brief review of diffusing wave spectroscopy, I describe in detail a new and more general method based on the transport/diffusion of correlation in optically dense systems.

4.2.1 Single Scattering

Consider the system depicted in fig. 4.2. A beam of coherent light is incident on a dilute suspension of identical scattering particles. The light scattered by an angle θ is detected by a photo-detector. The electric field reaching the detector is a superposition of all the scattered electric fields,

$$
\begin{aligned}
E &= E_o F(q) \sum_{n=1}^{N} \exp(i\mathbf{k_{in}} \cdot \mathbf{r}_n) \exp(i\mathbf{k_{out}} \cdot (\mathbf{R_d} - \mathbf{r}_n)) \\
&= E_o F(q) \exp(i\mathbf{k_{out}} \cdot \mathbf{R_d}) \sum_{n=1}^{N} \exp(-i\mathbf{q} \cdot \mathbf{r}_n) \ .
\end{aligned}
\tag{4.1}
$$

Here, E is the electric field reaching the detector at position $\mathbf{R_d}$, E_o is the amplitude of the incident field, and $F(q)$ is the form factor for light to receive a moment transfer of $\mathbf{q} = \mathbf{k_{out}} - \mathbf{k_{in}}$ where $\mathbf{k_{out}}$ and $\mathbf{k_{in}}$ are the output and input wavevectors respectively and $|\mathbf{q}| = 2k_o \sin \theta/2$ where $k_o = |k_{in}| = |k_{out}|$. For simplicity I neglect polarization effects and assume randomly positioned and oriented scatterers. Under these conditions the scattering differential cross-section is only dependent on the magnitude of $\mathbf{q}$. The summation is over the N particles in the scattering volume and $\mathbf{r}_n$ is the position of each particle. We see from eq. (4.1) that the phase of each scattered wave depends on the momentum transfer (i.e. scattering angle) and the position of the particle. In a disordered system, the particles are randomly distributed resulting in random constructive and destructive interference at the detector. Displacing a single particle changes the interference and thus the intensity reaching the detector.

For particles which are undergoing random relative motion, e.g. Brownian motion, the phases of the individual scattered waves are changing randomly, independently from the other scattered waves. The intensity at the detector will thus fluctuate. The time scale of the intensity fluctuations is given by the rate at which the phase of the scattered waves is changing and thus depends on the motion of the scattering particles and the momentum transfer. Therefore, the intensity fluctuations are more rapid at larger scattering angles and for faster moving particles.

By monitoring the intensity fluctuations it is possible to derive information about the motion of the scattering particles. There are two standard approaches. One entails analysis of the power spectrum of the detected signal, i.e.

$$S(\omega) = \int \mathrm{d}t I^2(t) \cos(\omega t) \ . \tag{4.2}$$

The other uses the unnormalized temporal autocorrelation of the intensity,

$$G_2(\tau) = \langle I(t) I(t + \tau) \rangle \ . \tag{4.3}$$

$I(t)$ is the intensity at time t and the $\langle ... \rangle$ denotes an ensemble average. For an ergodic system, an ensemble average is equivalent to a time average and thus $G_2(\tau)$ can be
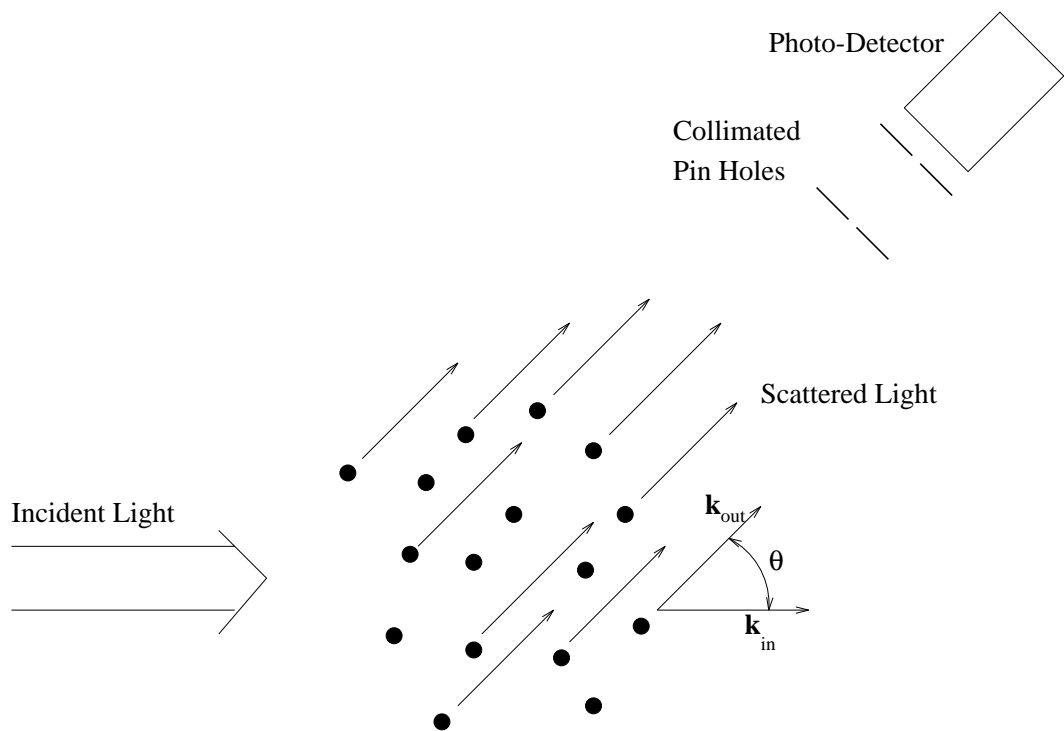
Figure 4.2: Light is incident on a dilute suspension of scatterers. The suspension is dilute enough such that photons are scattered no more than once. Light that is scattered by an angle θ is collimated by two pin-holes and monitored with a photo-detector.

obtained by a temporal average of the correlation function. The two methods are related as discussed [46, 52, 97, 98]. The exact relationship states that the intensity power spectrum and field correlation function form a Fourier transform pair [46, 98, 99, 100], i.e.

$$S(\omega) = \frac{\langle I \rangle^2}{2\pi} \int_{-\infty}^{\infty} \cos(\omega \tau) \left[g_2(\tau) - 1 \right] \, \mathrm{d}\tau \ , \tag{4.4}$$

where $g_2(\tau) = G_2(\tau) / \langle I \rangle^2$ is the normalized temporal intensity correlation function and $\langle I \rangle$ is the average intensity.

I focus on the temporal correlation method. Instead of calculating the temporal intensity autocorrelation function, $G_2(\tau)$, the standard approach is to derive the temporal field correlation function, $G_1(\tau) = \langle E(0) E^*(\tau) \rangle$, and note that the two are related by the Siegert relation [48, 50, 100]

$$G_2(\tau) = \langle I \rangle^2 + \beta |G_1(\tau)|^2 \ , \tag{4.5}$$

where $\langle I \rangle$ is the ensemble averaged intensity. β is a parameter which depends on the number of speckles detected and the coherence length and stability of the laser. β thus depends on the experimental setup. For an ideal experimental setup $\beta = 1$. See [101, 102] for more discussion on β.

The normalized temporal field correlation function is

$$g_1(\tau) = \frac{\langle E(0) E^*(\tau) \rangle}{\langle |E(0)|^2 \rangle} \ , \tag{4.6}$$

Using eq. (4.1) for the scattered electric field and noting that the cross terms resulting in eq. (4.6) average to zero when particle motions are uncorrelated, we find

$$g_1(\tau) = \langle \exp\left(i \mathbf{q} \cdot \Delta \mathbf{r}(\tau) \right) \rangle \ . \tag{4.7}$$

$\Delta \mathbf{r}(\tau) = \mathbf{r}(\tau) - \mathbf{r}(0)$ is the displacement of a particle in time τ and the average is over $\Delta \mathbf{r}(\tau)$ weighted by the appropriate distribution. In the case of Brownian motion, the average is weighted by [36]

$$P\left(\Delta \mathbf{r}(\tau)\right) = \frac{1}{(4\pi D_B \tau)^{3/2}} \exp\left(-\frac{|\Delta \mathbf{r}(\tau)|^2}{4 D_B \tau} \right) \ , \tag{4.8}$$

where $P\left(\Delta\mathbf{r}(\tau)\right)$ is the probability of a particle being displaced a distance $\Delta\mathbf{r}$ in a time τ. Calculating the weighted average, eq. (4.7) becomes

$$g_1(\tau) = \exp\left(-\frac{1}{6}q^2 \left\langle \Delta r^2(\tau) \right\rangle\right) \ . \tag{4.9}$$

$\left\langle \Delta r^2(\tau) \right\rangle = 6D_B\tau$ is the mean squared displacement of the scattering particles in time t where D_B is the Brownian diffusion coefficient. The correlation function thus decays exponentially with a decay time on the order of the amount of time it takes a scattering particle to move a wavelength of light. That is, the time scale of the intensity fluctuations is on the order of the time it takes a particle to move one light wavelength $\left(q^{-1}\right)$.

The decay of $g_1(\tau)$ for systems with random flow can also be calculated. In this case $\Delta\mathbf{r}(\tau) = \mathbf{V}\tau$ and the average is over the velocity distribution. For an isotropic, Gaussian velocity distribution, the correlation function still decays as eq. (4.9) but $\left\langle \Delta\mathbf{r}(\tau)^2 \right\rangle = \left\langle \Delta V^2 \right\rangle \tau^2$ where $\left\langle \Delta V^2 \right\rangle$ is the mean square velocity. A Gaussian speed distribution is assumed [103]. Shear flow and turbulence have also been studied [40, 41, 42, 43, 104].

4.2.2   Multiple Scattering - Diffusing Wave Spectroscopy

When the concentration of scattering particles is increased, light is scattered many times before it exits the system (see fig. 4.3). The photons reaching the detector have followed various trajectories of differing path lengths. Under these conditions the correlation function can be calculated using the framework of diffusing wave spectroscopy (DWS). Considering only those photons which have scattered N times before detection, the normalized field correlation function has the form

$$\begin{aligned}
g_1^{(N)}(\tau) &= \left\langle \exp\left(i\sum_{n=1}^{N} \mathbf{q}_n \cdot \Delta\mathbf{r}_n\right)\right\rangle_{q,\Delta\mathbf{r}} \\
&= \left\langle \exp\left(i\mathbf{q}\cdot\Delta\mathbf{r}\right)\right\rangle_{q,\Delta\mathbf{r}}^{N} \\
&= \left\langle \exp\left(-\frac{1}{6}q^2\left\langle \Delta r^2(\tau)\right\rangle\right)\right\rangle_{q}^{N}
\end{aligned}$$

$$= \exp\left(-\frac{1}{6}\left\langle q^2\right\rangle\left\langle\Delta r^2(\tau)\right\rangle s/l\right) \ . \tag{4.10}$$

On the first line the sum appears in the argument of the exponent to account for the phase shift accumulated from each scattering event. The $\langle...\rangle$ denotes an average over the momentum transfer and particle displacement. The average over the scattering angle (momentum transfer) is necessary because it is not constrained as it was in the single scattering experiment. The second line is derived assuming that successive scattering events and neighboring particle motions are uncorrelated. These assumptions are valid in a disordered system with no particle-particle interactions. Some care must be taken when particle motions are correlated. The third line results from the ensemble average over the particle displacement where $\langle\Delta r^2(\tau)\rangle$ is the mean square displacement of the scattering particles (see section 4.2.1). The mean-square displacement has been assumed to be isotropic. This is the case with Brownian motion and random flow, but not directional flows. We next bring the q-average inside the argument of the exponential via a first order cummulant expansion. This approximation is valid as long as $\frac{1}{6}q^2\langle\Delta r^2(\tau)\rangle \ll 1$. Finally we assume that there have been many scattering events in which case N is well approximated by s/l where s is the path length and $l = 1/\mu_s$ is the scattering length.

The average over the momentum transfer is weighted by the normalized differential cross section. That is

$$
\begin{aligned}
\left\langle q^2\right\rangle &= \int_0^\pi f(\cos\theta)q^2\mathrm{d}(\cos\theta) \\
&= 4k_o^2\left\langle\sin^2\frac{\theta}{2}\right\rangle \\
&= 2k_o^2\left[1 - \langle\cos\theta\rangle\right] \\
&= 2k_o^2\frac{l}{l^*} \ . \tag{4.11}
\end{aligned}
$$

Here $f(\cos\theta)$ is the normalized form factor and $q^2 = 4k_o^2\sin^2(\theta/2)$. Using the similarity relation discussed in section 2.1 we see that $l/l^* = 1 - \langle\cos\theta\rangle$, where $l^* = 1/\mu_s'$ is the photon random walk step length and the average over $\cos\theta$ is also weighted by the normalized differential cross-section, we see that $\langle q^2\rangle = 2k_o^2 l/l^*$. Therefore,
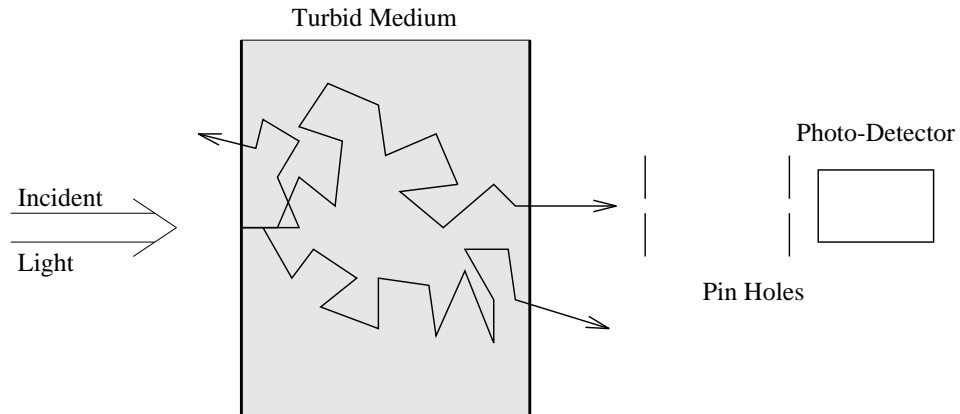
Figure 4.3: Light is incident on a concentrated suspension of scatterers. Photons on average are scattered many times before exiting the system. A single speckle of transmitted light is imaged with pin holes (or gathered by a single-mode fiber) and monitored with a photo-detector.

the normalized field correlation function of light that has migrated a path length s through a highly scattering system is given by

$$g_1^{(N)}(\tau) = \exp\left(-\frac{1}{3}k_o^2\left\langle\Delta r^2(\tau)\right\rangle\frac{s}{l^*}\right) \; . \tag{4.12}$$

Eq. (4.12) has the same form as the single scattering result, eq. (4.9), except the decay rate is multiplied by the number of random walk steps in the medium, s/l^*, and k_o appears instead of q because there is no longer a single scattering angle in the problem. The correlation function for trajectories of longer length will decay more quickly, permitting the motion of scattering particles to be probed on ever shorter time scales.

The validity of eq. (4.12) has been verified directly by Yodh *et al.* [105] using a pulsed laser and gating the broadened response to select photon path lengths of a specific length. A summary of their experimental results is shown in fig. 4.4. They measured the correlation function for photon path lengths between 7 cm and 13 cm through a 2.0 mm thick 30% suspension of 0.460 μm polystyrene spheres. In the inset of fig. 4.4 they demonstrate the single exponential decay of the correlation function for two different path lengths. Fig. 4.4 shows that the decay rate increases linearly with
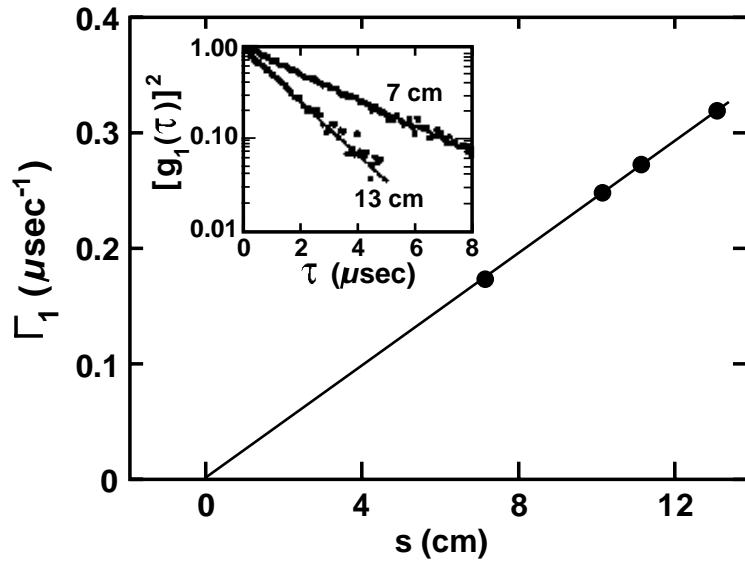
Figure 4.4: The decay rate for the correlation function increases linearly with the photon path length. The correlation function measured for photon path lengths of 7 cm and 13 cm is shown in the inset. The decay is log-linear as expected. Reproduced with permission from A. G. Yodh *et al.* Phys. Rev. B **42**, 4744 (1990) [105].

the path length as expected by eq. (4.12).

It is not always convenient to use a pulsed laser and gating techniques to pick out photons which have traveled a specific path length through the sample. Generally, a continuous wave laser is used to illuminate the sample and the full distribution of path lengths contributes to the decay of the correlation function. Under these conditions, the field correlation function is given by

$$g_1(\tau) = \int_0^\infty P(s) \exp\left(-\frac{1}{3}k_o^2 \left\langle \Delta r^2(\tau) \right\rangle \frac{s}{l^*}\right) ds \; , \qquad (4.13)$$

where $P(s)$ is the normalized distribution of path lengths. This relation is valid given the assumption that the laser coherence length is much longer than the width of the photon path length distribution [102]. When the scattering length is much smaller than the dimensions of the sample and the absorption length, the path length distribution is found from the photon diffusion equation. For a point source and point detector in

an infinite medium, $P(s)$ is

$$P(s) = \sqrt{\frac{vr_{sd}^2}{4\pi D}} \exp\left(\sqrt{\frac{v\mu_a r_{sd}^2}{D}}\right) s^{-3/2} \exp\left(-\frac{vr_{sd}^2}{4Ds}\right) \exp\left(-\mu_a s\right) . \qquad (4.14)$$

Here r_{sd} is the separation between the source and detector. Using the photon diffusion approximation to calculate $P(s)$, $g_1(\tau)$ has been calculated for various geometries including semi-infinite and slab [106]. The solution for an infinite medium with a point source is

$$g_1(\tau) = \exp\left(-\sqrt{k_o^2 \langle \Delta r^2(\tau)\rangle + 3\mu_a l^*} \ \frac{r_{sd}}{l^*}\right) . \qquad (4.15)$$

With no photon-absorption, the correlation function still decays as a single exponential but as the $\sqrt{\langle \Delta r^2(\tau)\rangle}$ instead of as $\langle \Delta r^2(\tau)\rangle$. Photon absorption reduces the contribution of long path length photons and thus suppresses the decay at early correlation times. $g_1(\tau)$ has been verified experimentally for absorption free media by Pine *et al.* [106] and for absorbing media by Tamura and co-workers [107, 108].

For a semi-infinite medium with a collimated point source and a point detector, the distribution of photon path lengths is found using the method of images to satisfy the semi-infinite boundary condition (see section 2.3). The photon path length distribution is

$$P(s) = \left[\sqrt{\frac{4\pi D}{vr_1^2}} \exp\left(-\sqrt{\frac{v\mu_a r_1^2}{D}}\right) - \sqrt{\frac{4\pi D}{vr_2^2}} \exp\left(-\sqrt{\frac{v\mu_a r_2^2}{D}}\right)\right]^{-1}$$
$$s^{-3/2} \left[\exp\left(-\frac{vr_1^2}{4Ds}\right) - \exp\left(-\frac{vr_2^2}{4Ds}\right)\right] \exp\left(-\mu_a s\right) . \qquad (4.16)$$

The distance from the real source to the detector is $r_1 = (\rho^2 + l^{*2})^{1/2}$ where ρ is the separation between the source and detector on the surface and l^* is the distance inside the medium where the collimated source becomes diffuse. The distance between the image source and the detector is $r_2 = (\rho^2 + (l^* + 2z_b)^2)^{1/2}$ where z_b is the extrapolation distance to the imaging boundary as determined by the mismatch in the indices of

refraction (see section 2.3). With this $P(s)$ the field correlation function is

$$g_1(\tau) = \frac{\exp\left(-\sqrt{k_o^2 \langle \Delta r^2(\tau) \rangle + 3\mu_a l^*} \ \frac{r_1}{l^*}\right) - \exp\left(-\sqrt{k_o^2 \langle \Delta r^2(\tau) \rangle + 3\mu_a l^*} \ \frac{r_2}{l^*}\right)}{\exp\left(-\sqrt{3\mu_a l^*} \ \frac{r_1}{l^*}\right) - \exp\left(-\sqrt{3\mu_a l^*} \ \frac{r_2}{l^*}\right)} \ .$$

(4.17)

Other important geometries include plane wave transmission through a slab and diffuse backscattering of a plane wave. These solutions are discussed by Pine *et al.* [106]. For plane wave transmission through a slab

$$g_1(\tau) = \frac{\left(\frac{L}{l^*} + \frac{4}{3}\right)\sqrt{6D_B k_o^2 \tau}}{\left(1 + \frac{8}{3}D_B k_o^2 \tau\right)\sinh\left[\frac{L}{l^*}\sqrt{6D_B k_o^2 \tau}\right] + \frac{4}{3}\sqrt{6D_B k_o^2 \tau}\cosh\left[\frac{L}{l^*}\sqrt{6D_B k_o^2 \tau}\right]} \ ,$$

(4.18)

where L is the thickness of the slab. For backscattering of a plane wave from a slab

$$g_1(\tau) = \frac{\sinh\left[\sqrt{6D_B k_o^2 \tau}\left(\frac{L}{l^*} - 1\right)\right] + \frac{2}{3}\sqrt{6D_B k_o^2 \tau}\cosh\left[\sqrt{6D_B k_o^2 \tau}\left(\frac{L}{l^*} - 1\right)\right]}{\left(1 + \frac{8}{3}D_B k_o^2 \tau\right)\sinh\left[\frac{L}{l^*}\sqrt{6D_B k_o^2 \tau}\right] + \frac{4}{3}\sqrt{6D_B k_o^2 \tau}\cosh\left[\frac{L}{l^*}\sqrt{6D_B k_o^2 \tau}\right]} \ .$$

(4.19)

For a slab of infinite thickness, eq. (4.19) becomes

$$g_1(\tau) = \frac{\exp\left[-\sqrt{6D_B k_o^2 \tau}\right]}{1 + \frac{2}{3}\sqrt{6D_B k_o^2 \tau}} \ .$$

(4.20)

To summarize, within the framework of diffusing wave spectroscopy, the decay of $g_1(\tau)$ is found by first considering photon trajectories of a given length through the sample and calculating the average phase fluctuations by averaging over the particle displacements and the momentum transfer per scattering event. The distribution of path lengths through the sample is then used to determine the overall decay of $g_1(\tau)$.

Similar equations for the field correlation function arising from highly scattering systems have been obtain using field theory. For discussions on the derivation using field theory see MacKintosh and John [49], Maret and Wolf [50], and Vol'kov and Romanov [51].

4.2.3 Correlation Transport and Correlation Diffusion

A different approach for finding $g_1(\tau)$ has been proposed by Ackerson *et al.* [57, 58] that does not rely on the assumptions made by DWS. This new approach treats the

transport of correlation through a scattering system much like the radiative transport equation [60, 83] treats the transport of photons. The difference between the correlation transport equation (CT) and the radiative transport equation (RT) is that the CT accumulates the decay of the correlation function for each scattering event. Since contributions to the decay of the correlation function arise from each scattering event from a moving particle, the CT is simply constructed by adding the single scattering correlation function to the term which accounts for photon scattering in the RT equation (eq. (2.1)). This term accounts for all scattering events. The correlation transport equation is thus [57, 58]

$$\nabla \cdot G_1^T(\mathbf{r}, \hat{\Omega}, \tau)\hat{\Omega} + \mu_t G_1^T(\mathbf{r}, \hat{\Omega}, \tau) = \mu_s \int G_1^T(\mathbf{r}, \hat{\Omega}', \tau)g_1^s(\hat{\Omega}, \hat{\Omega}', \tau)f(\hat{\Omega}, \hat{\Omega}')\mathrm{d}\hat{\Omega}' + S(\mathbf{r}, \hat{\Omega}) \ .$$
$$(4.21)$$

Here, $G_1^T(\mathbf{r}, \hat{\Omega}, \tau)$ is the unnormalized temporal field correlation function which is a function of position $\mathbf{r}$, direction $\hat{\Omega}$, and correlation time τ. The scattering and absorption coefficients are respectively μ_s and μ_a, and $\mu_t = \mu_s + \mu_a$. $g_1^s(\hat{\Omega}, \hat{\Omega}', \tau)$ is the normalized temporal field correlation function for single scattering. $f(\hat{\Omega}, \hat{\Omega}')$ is the normalized differential scattering cross-section. $S(\mathbf{r}, \hat{\Omega})$ is the light source distribution. The scattering coefficient is the reciprocal of the scattering length, $\mu_s = 1/l$, and the absorption coefficient is the reciprocal of the absorption length, $\mu_a = 1/l_a$. The time dependence (not to be confused with correlation time) has been left out of the equation since I only consider measurements with CW sources and systems in equilibrium (i.e. steady state). The time dependence can be included by adding a time-derivative of $G_1^T(\mathbf{r}, \hat{\Omega}, \tau)$ (i.e. $v^{-1}\frac{\partial}{\partial t}G_1^T(\mathbf{r}, \hat{\Omega}, \tau, t)$) to the left-hand side of eq. (4.21) and letting $G_1^T(\mathbf{r}, \hat{\Omega}, \tau) \rightarrow G_1^T(\mathbf{r}, \hat{\Omega}, \tau, t)$.

At zero correlation time, $\tau = 0$, there has been no decorrelation and the CT equation reduces to the RT equation. This equivalence arises because the unnormalized field correlation function at $\tau = 0$ is just the ensemble averaged intensity, which is the quantity determined by the RT equation.

The CT equation provides a means for considering the intermediate regime between single scattering systems and systems through which light diffuses. Furthermore, in

the limit of single scattering, it reduces to the standard single scattering correlation function discussed in section 4.2.1 and, as I will discuss, solutions in the photon diffusion regime are the same as obtained from DWS (see section 4.2.2). The CT equation is useful because its validity ranges from single scattering to multiple scattering systems, does not require the assumptions made within DWS, and affords a straight-forward approach to considering systems with spatially-varying optical and dynamical properties. A drawback to the CT equation is the difficulty in obtaining analytical and numerical solutions. The RT equation is plagued by the same problem. Because of the similarity between the CT equation and the RT equation we should be able to apply the same approximation methods to the CT equation as we applied to the RT equation.

Using the standard diffusion approximation the CT equation reduces to the following correlation diffusion equation (see appendix A):

$$\left(D_\gamma \nabla^2 - v\mu_a - \frac{1}{3}v\mu_s' k_o^2 \left\langle \Delta r^2(\tau) \right\rangle \right) G_1(\mathbf{r}, \tau) = -vS(\mathbf{r}) . \qquad (4.22)$$

Here, $D_\gamma = v/(3\mu_s')$ is the photon diffusion coefficient, v is the speed of light in the medium, and $\mu_s' = \mu_s(1 - \langle \cos\theta \rangle) = 1/l^*$ is the reduced scattering coefficient. Recall that for Brownian motion $\left\langle \Delta r^2(\tau) \right\rangle = 6D_B\tau$ and for random flow $\left\langle \Delta r^2(\tau) \right\rangle = \left\langle \Delta V^2 \right\rangle \tau^2$.

To obtain the correlation diffusion equation it is necessary to assume that the photons are diffusing and that the scattering phase function, $f(\hat{\Omega}, \hat{\Omega}')$, and the single scattering correlation function, $g_1^s(\hat{\Omega}, \hat{\Omega}', \tau)$, only depend on the scattering angle $\hat{\Omega} \cdot \hat{\Omega}'$, and that $k_o^2 \left\langle \Delta r^2(\tau) \right\rangle \ll 1$. The photon diffusion assumption is valid if the photon random walk step length is smaller than the dimensions of the sample and the photon absorption length. The scattering angle assumption (i.e. $\hat{\Omega} \cdot \hat{\Omega}'$) is valid for systems with randomly oriented scatterers and isotropic dynamics (e.g. Brownian motion and random flow). The short time assumption requires the correlation time τ to be much smaller than the time it takes a scatterer to move a wavelength of light. When the photon wavelength is 514 nm and the dynamics are Brownian motion with $D_B = 1\mathrm{x}10^{-8}$ cm^{2}s^{-1}, then the short time assumption requires $\tau \ll 1\mathrm{x}10^{-3}$ s. The

breakdown of this approximation is explored in section 4.4. In an infinite, homogeneous system the breakdown of this approximation is observable at 225 μs and is independent of the photon absorption coefficient. The deviation increases with source-detector separation and reduced scattering coefficient. For a source-detector separation of 1 cm the deviation is 20% and increases to 100% for a 2 cm source-detector separation.

Eq. (4.22) can be recast as a Helmholtz equation for the field correlation function, i.e.

$$\left(\nabla^2 + K^2(\tau)\right) G_1(\mathbf{r}, \tau) = -\frac{vS}{D_\gamma}\delta^3(\mathbf{r} - \mathbf{r_s}) \ , \tag{4.23}$$

where $K^2(\tau) = -v\left(\mu_a + \frac{1}{3}\mu_s' k_o^2 \left\langle \Delta r^2(\tau)\right\rangle\right)/D_\gamma$. Here I have taken the light source to be point like, i.e. CW, and located at position $\mathbf{r_s}$. Note that $\frac{1}{3}\mu_s' k_o^2 \left\langle \Delta r^2(\tau)\right\rangle$ is a loss term similar to μ_a. While μ_a represents losses due to photon absorption, $\frac{1}{3}\mu_s' k_o^2 \left\langle \Delta r^2(\tau)\right\rangle$ represents the "absorption" of correlation due to dynamic processes. When $\tau = 0$ there is no dynamic absorption and eq. (4.23) reduces to the steady-state photon diffusion equation (eq. (2.12)).

For an infinite, homogeneous system with no photon absorption (i.e. $\mu_a = 0$), the solution to eq. (4.23) has the well known form

$$G_1(\mathbf{r}, \tau) = \frac{vS \exp\left(-\sqrt{\mu_s'^2 k_o^2 \left\langle \Delta r^2(\tau)\right\rangle} \ |\mathbf{r} - \mathbf{r_s}|\right)}{4\pi D_\gamma |\mathbf{r} - \mathbf{r_s}|} \ . \tag{4.24}$$

This same solution has been derived within the context of DWS [48, 50], and from the scalar wave equation for the electric field propagating in a medium with a fluctuating dielectric constant [49, 109]. In contrast to these two approaches, the correlation diffusion equation provides a simple framework for considering turbid media with large scale spatially varying dynamics and optical properties.

With some difficulty, such systems can be considered with diffusing-wave spectroscopy. I have considered this and found that diffusing-wave spectroscopy requires the computation of complicated integrations of photon dwell times in localized voxels convolved with a volume integral. On the other hand, the correlation diffusion equation requires the solution of a simple differential equation. Because the correlation

diffusion equation is analogous to the photon diffusion equation, we can apply all of the techniques developed for photon diffusion to correlation diffusion. In the next few sections I demonstrate the "scattering" of correlation from dynamical inhomogeneities as well as tomographic reconstructions of the spatially varying dynamical properties of turbid media.

4.2.4   Ergodicity

The samples that I study experimentally are not ergodic, that is the time-averaged measurements are not equivalent to the ensemble-average computed by the various photon correlation spectroscopy theories. Ultimately this situation arises whenever the sample has static and dynamic scattering components. This presents a problem when measuring the temporal intensity correlation function $g_2(\tau)$ but is not a problem if one is measuring the temporal field correlation function $g_1(\tau)$ directly. To see the origin of the problem, it is necessary to begin with the electric field emerging from a non-ergodic system and derive $g_1(\tau)$ and $g_2(\tau)$.

The following discussion assumes that the non-ergodic system is highly scattering and comprises two components, a static, non-ergodic component and a dynamic, ergodic component. The extension to dynamic but non-ergodic systems is relatively straightforward but not relevant to this dissertation. Discussions of such systems can be found in [110, 111].

The electric field reaching the detector is a superposition of photons that have migrated through the static region without scattering from moving particles and photons that have scattered at least once from a moving (dynamic) particle. I refer to these two different types of photons as "constant" and "fluctuating." Thus,

$$E(t) = E_c(t) + E_f(t) \tag{4.25}$$

where

$$E_c(t) = \sum_{i=1}^{N_c} \varepsilon_c^i(t) \tag{4.26}$$

is the constant electric field reaching the detector and

$$E_f(t) = \sum_{i=1}^{N_f} \varepsilon_f^i(t) \tag{4.27}$$

is the fluctuating electric field reaching the detector. The sum for $E_c(t)$ is over the number of photon trajectories (N_c) that travel only in the static region between the source and detector, where $\varepsilon_c^i(t)$ is the field for the ith photon trajectory. The sum for $E_f(t)$ is over the number of photon trajectories (N_f) that sample the dynamic region between the source and detector, where $\varepsilon_f^i(t)$ is the field for the ith photon trajectory.

With these definitions, the temporal electric field correlation function is

$$
\begin{aligned}
g_1(\tau) &= \frac{\langle E(t) E^*(t+\tau) \rangle_t}{\langle |E|^2 \rangle_t} \\
&= \frac{\langle E_c(t) E_c^*(t+\tau) \rangle_t + \left\langle E_f(t) E_f^*(t+\tau) \right\rangle_t}{I_c + \langle I_f \rangle + \left\langle E_c(t) E_f^*(t) \right\rangle_t + \langle E_f(t) E_c^*(t) \rangle_t} \\
&\quad + \frac{\left\langle E_c(t) E_f^*(t+\tau) \right\rangle_t + \langle E_f(t) E_c^*(t+\tau) \rangle_t}{I_c + \langle I_f \rangle + \left\langle E_c(t) E_f^*(t) \right\rangle_t + \langle E_f(t) E_c^*(t) \rangle_t} \\
&= \left[\frac{I_c + \langle I_f \rangle \, g_{1,f}(\tau)}{I_c + \langle I_f \rangle} \right] .
\end{aligned}
\tag{4.28}
$$

The $\langle ... \rangle_t$ denotes a time average. E_c does not fluctuate in time and thus the intensity $I_c = \langle E_c(t) E_c^*(t+\tau) \rangle_t$ is constant. $E_f(t)$ does fluctuate in time so that $\langle I_f \rangle = \left\langle E_f(t) E_f^*(t) \right\rangle_t$ is the time-averaged fluctuating intensity and $g_{1,f}(\tau)$ is the temporal field correlation function of $E_f(t)$ (this decays from 1 to 0). The terms in the numerator on the third line in eq. (4.28) average to zero because the phases of the constant and fluctuating photon trajectories are uncorrelated. Likewise, the third and fourth terms in the denominator on the second and third lines average to zero.

Eq. (4.28) is the field correlation function which we calculate using the correlation diffusion equation. If more than one speckle is imaged with the collection optics then a coherence parameter $\sqrt{\beta}$ enters to reduce the observed decay of $g_1(\tau)$. Under these less than ideal conditions the measured correlation function is

$$g_1(\tau) = \left[\frac{I_c + \sqrt{\beta} \langle I_f \rangle \, g_{1,f}(\tau)}{I_c + \langle I_f \rangle} \right] . \tag{4.29}$$

The factor $\sqrt{\beta}$ is easily removed from $g_1(\tau)$. The field correlation function is expected to decay from 1 and plateau at a value of $B = I_c/(I_c + \langle I_f \rangle)$. The less than ideal experimental conditions will result in $g_1(\tau)$ decaying from a value less than 1 to B. In non-ideal conditions, the total decay will be $\sqrt{\beta}\, A = \sqrt{\beta}\, \langle I_f \rangle /(I_c + \langle I_f \rangle)$, when it was expected to be A. $A + B = 1$, and B is found from the value of $g_1(\tau)$ as $\tau \to \infty$. We can thus obtain the correct field correlation function using

$$g_1^{\text{Correct}}(\tau) = (1 - B)\frac{g_1^{\text{Measured}}(\tau) - B}{g_1^{\text{Measured}}(\tau = 0) - B} + B \ . \qquad (4.30)$$

As we will see, problems arise when measuring $g_2(\tau)$ because the value of B and A cannot be determined.

Deriving the explicit form for the temporal intensity correlation function is a little more involved. In this case

$$\begin{aligned}
G_2(\tau) &= \langle I(t)I(t + \tau) \rangle_t \\
&= \langle E(t)E^*(t)E(t + \tau)E^*(t + \tau) \rangle_t \\
&= I_c^2 + I_c(t)\langle I_f \rangle + E_c(t)E_c^*(t + \tau)\left\langle E_f^*(t)E_f(t + \tau) \right\rangle_t \\
&\quad + E_c^*(t)E_c(t + \tau)\left\langle E_f(t)E_f^*(t + \tau) \right\rangle_t + \langle I_f \rangle I_c(\tau) \\
&\quad + \left\langle E_f(t)E_f^*(t)E_f(t + \tau)E_f^*(t + \tau) \right\rangle \ .
\end{aligned} \qquad (4.31)$$

The product on the first line of eq. (4.31) results in 16 terms, 10 of which average to zero. The remaining 6 terms are given on the 3rd, 4th, and 5th lines. Although E_c and I_c are independent of time, the argument is given to indicate the origin of the different terms. The 3rd and 4th terms are the heterodyne terms arising from the beating of E_c with $E_f(t)$, i.e.

$$E_c(t)E_c^*(t+\tau)\left\langle E_f^*(t)E_f(t + \tau) \right\rangle_t = E_c^*(t)E_c(t+\tau)\left\langle E_f(t)E_f^*(t + \tau) \right\rangle_t = I_c \langle I_f \rangle g_{1,f}(\tau) \ . \qquad (4.32)$$

The 6th term is more complicated. The summations over different trajectories giving rise to $E_f(t)$ (eq. (4.27)) must be included and the time-average of the products

of the different trajectories must be considered. The 6th term is thus

$$\left\langle E_f(t)E_f^*(t)E_f(t+\tau)E_f^*(t+\tau)\right\rangle_t = \sum_{i,j,k,l=1}^{N_f} \left\langle \varepsilon_f^i(t)\varepsilon_f^{j*}(t)\varepsilon_f^k(t+\tau)\varepsilon_f^{l*}(t+\tau)\right\rangle_t$$

$$= \sum_{i=j=k=l=1}^{N_f} \left\langle \varepsilon_f^i(t)\varepsilon_f^{j*}(t)\varepsilon_f^k(t+\tau)\varepsilon_f^{l*}(t+\tau)\right\rangle_t$$

$$+ \sum_{i=j=1,k=l=1,i\neq k}^{N_f} \left\langle \varepsilon_f^i(t)\varepsilon_f^{j*}(t)\varepsilon_f^k(t+\tau)\varepsilon_f^{l*}(t+\tau)\right\rangle_t$$

$$= \langle I_f\rangle^2 + \langle I_f\rangle^2 \left[\frac{N_f^2 - N_f}{N_f^2}\right]|g_{1,f}(\tau)|^2$$

$$\approx \langle I_f\rangle^2 + \langle I_f\rangle^2 |g_{1,f}(\tau)|^2 \ . \tag{4.33}$$

The first term, $\langle I_f\rangle^2$, derives from the N_f, $i = j$ terms multiplied by the N_f, $k = l$ terms. The second term results from $i = l$ and $j = k$, excluding the N_f terms where $i = j = k = l$. The reasonable assumption $N_f \ll N_f^2$ is made. The other combinations of i, j, k, and l average to zero because the phases are uncorrelated.

The temporal intensity correlation function for the described non-ergodic system is thus

$$g_2(\tau) = 1 + \frac{2\sqrt{\beta}\ I_c \langle I_f\rangle |g_{1,f}(\tau)| + \beta \langle I_f\rangle^2 |g_{1,f}(\tau)|^2}{(I_c + \langle I_f\rangle)^2} \ . \tag{4.34}$$

This correlation function has a heterodyne term, $2I_c \langle I_f\rangle |g_{1,f}(\tau)|$, and a homodyne term, $\langle I_f\rangle^2 |g_{1,f}(\tau)|^2$. I have included the coherence factor β which depends on the number of speckles averaged and the laser coherence length. When measuring a single speckle created by a stable, long coherence length laser, then $\beta = 1$. Unfortunately, experimentally, β usually varies between 0 and 1 and must be measured. It is safe to assume that β will remain constant for measurements made on different speckles since β only depends on the laser and detection optics. However I_c will vary, changing the relative importance of the homodyne and heterodyne terms.

The standard method to obtain the field correlation function (that which we calculate) from the intensity correlation function (that which we measure) is to use the Siegert relation

$$g_2(\tau) = 1 + \beta|g_1(\tau)|^2 \ . \tag{4.35}$$

This method does not work when the system is non-ergodic. If we determine $g_1(\tau)$ from the measured $g_2(\tau)$ (eq. (4.34)) using eq. (4.35) then we find that

$$g_1(\tau) = \left[\frac{2\sqrt{\beta} I_c \langle I_f \rangle \, |g_{1,f}(\tau)| + \beta \langle I_f \rangle^2 \, |g_{1,f}(\tau)|^2}{2\sqrt{\beta} \, I_c \langle I_f \rangle + \beta \langle I_f \rangle^2} \right]^{1/2} . \tag{4.36}$$

Not only is this different than what we calculate (eq. (4.28)), but many different $g_1(\tau)$'s could be measured for the same system by changing the experimental setup and thus changing β and/or by imaging a different speckle and thus changing I_c. Even if β were known (say $\beta = 1$), this method would not produce the correct field correlation function. Furthermore, $g_1(\tau)$ determined in this way decays from 1 to 0 when it should decay from 1 to B.

The standard approach for obtaining $g_1(\tau)$ from $g_2(\tau)$ thus does not apply to non-ergodic systems. Another approach has been suggested by Joosten *et al.* [112]. Their approach is to make the measurement on a speckle where the intensity is the ensemble-averaged intensity. The fluctuating part of the correlation function is then correct and the correct correlation function is obtained by adding a constant to $g_2(\tau)$ so that it decays from 2 to a value greater than 1 instead of decaying from a value less than 2 to 1. Assuming $\beta = 1$ then the value added to $g_2(\tau)$ is just B^2, such that

$$\begin{aligned}
g_2(\tau) &= 1 + \frac{\beta I_c^2 + 2\sqrt{\beta} \; I_c \langle I_f \rangle \, |g_{1,f}(\tau)| + \beta \langle I_f \rangle^2 \, |g_{1,f}(\tau)|^2}{(I_c + \langle I_f \rangle)^2} \\
&= 1 + \beta \frac{(I_c + \langle I_f \rangle \, |g_{1,f}(\tau)|)^2}{(I_c + \langle I_f \rangle)^2} .
\end{aligned} \tag{4.37}$$

The correct $g_1(\tau)$ can then be calculated using the Siegert relation (eq. (4.35)). The disadvantage of this method is that β must be known and the measurement must be made on an appropriate speckle. It is possible to determine β using an ergodic system but experience will show that for a fixed source and detection system that β can vary by up to 10% over the course of a few minutes. Furthermore, collecting light from a specific speckle emanating from a turbid medium for more than a few seconds requires extreme measures to isolate the system from mechanical vibrations. Joosten's *et al* method is therefore not practical if an accuracy better than 10% is desired.
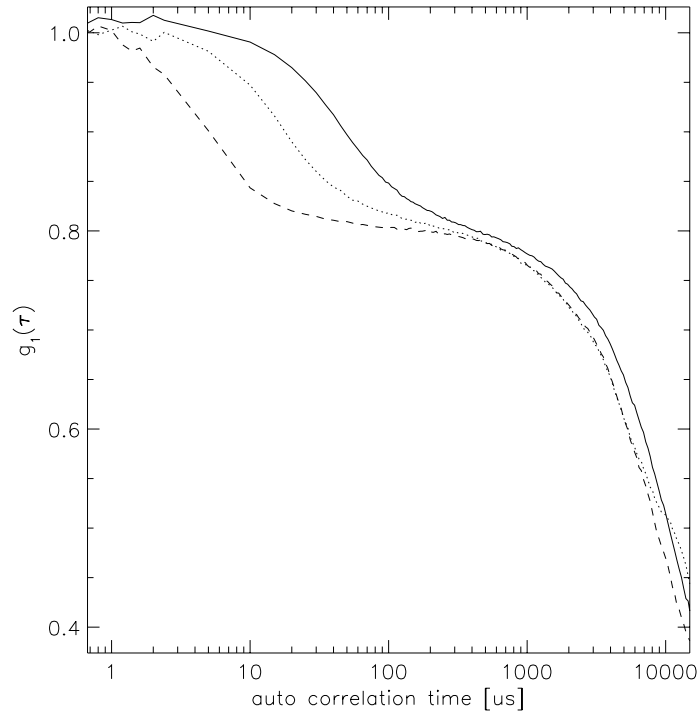
Figure 4.5: The ensemble average correlation function from a non-ergodic turbid medium is shown. The medium is a solid, highly scattering slab with a cylindrical vein through which a highly scattering colloid flows. The early τ decay corresponds to the flow dynamics while the long τ decay results from the ensemble averaging. The three curves come from three different flow speeds, the solid/dotted/dashed lines correspond to flow speeds of $0.08/0.24/0.88$ cm s^{-1} respectively. The early τ decay rate increases with the flow speed. The longer τ decay depends only on the rate of ensemble averaging, which is held constant. The intermediate plateau reveals the relative magnitudes of $\langle I_c \rangle$ and $\langle I_f \rangle$ and tells us what fraction of the detected photons have sampled the dynamic region. This is independent of the flow speed as expected.

In general, for a non-ergodic system, from a measurement of $g_2(\tau)$ it is not possible to independently determine I_c, $\langle I_f \rangle$, and β. Therefore the proper temporal electric field correlation function cannot be determined. In order to obtain the proper correlation function I ensemble average during the acquisition of the intensity correlation function. This method has been described in detail by Xue *et al.* [110]. The technique for ensemble averaging that I use is explained in section 6.2. Basically, the idea is to move the detector from speckle to speckle during the course of the measurement. In this way, $E_c(t)$ will fluctuate on a time scale given by the motion of the detector from speckle to speckle. Eq. (4.31) thus becomes

$$
\begin{aligned}
G_2(\tau) &= \left\langle E_c(t) E_c^*(t) E_c(t+\tau) E_c^*(t+\tau) \right\rangle + \left\langle E_c(t) E_c^*(t+\tau) \right\rangle \left\langle E_f^*(t) E_f(t+\tau) \right\rangle \\
&\quad + \left\langle E_c^*(t) E_c(t+\tau) \right\rangle \left\langle E_f(t) E_f^*(t+\tau) \right\rangle + 2 \left\langle I_f \right\rangle \left\langle I_c \right\rangle \\
&\quad + \left\langle E_f(t) E_f^*(t) E_f(t+\tau) E_f^*(t+\tau) \right\rangle \\
&= \left(\langle I_c \rangle + \langle I_f \rangle \right)^2 + \beta \left(\langle I_c \rangle \left| g_{1,c}(\tau) \right| + \langle I_f \rangle \left| g_{1,f}(\tau) \right| \right)^2 ,
\end{aligned}
\tag{4.38}
$$

where $\langle I_c \rangle$ is the average intensity of the constant component of the speckles, $g_{1,c}(\tau)$ is the correlation function of the fluctuating $E_c(t)$, and all $\langle ... \rangle$ are time averages. The normalized intensity correlation function is thus

$$
g_2(\tau) = 1 + \beta \frac{\left(\langle I_c \rangle \left| g_{1,c}(\tau) \right| + \langle I_f \rangle \left| g_{1,f}(\tau) \right| \right)^2}{\left(\langle I_c \rangle + \langle I_f \rangle \right)^2} .
\tag{4.39}
$$

$g_{1,c}(\tau)$ decays in a log-linear fashion on a time scale that is proportional to the amount of time it takes to move the detector from one speckle to the next [111]. If the decay time of $g_{1,c}(\tau)$ is much longer than that of $g_{1,f}(\tau)$ then the measured correlation function will look like that shown in fig. 4.5 and the fluctuations due to sample dynamics are easily separated from ensemble averaging fluctuations. The correlation function at early times when $g_{1,c}(\tau) \approx 1$ is then

$$
g_2(\tau) = 1 + \beta \frac{\left(\langle I_c \rangle + \langle I_f \rangle \left| g_{1,f}(\tau) \right| \right)^2}{\left(I_c + \langle I_f \rangle \right)^2} ,
\tag{4.40}
$$

and from the Siegert relation [48, 50, 100]

$$
g_2(\tau) = 1 + \beta |g_1(\tau)|^2
\tag{4.41}
$$

we find that

$$g_1(\tau) = \frac{(\langle I_c \rangle + \langle I_f \rangle \, |g_{1,f}(\tau)|)}{(\langle I_c \rangle + \langle I_f \rangle)} \, . \tag{4.42}$$

This is exactly the temporal field correlation function which we calculate with the correlation diffusion theory. There is no need to separate $\langle I_f \rangle \, |g_{1,f}(\tau)|$ from $\langle I_c \rangle$. From the plateau in the correlation function that occurs when $g_{1,f}(\tau) \ll 1$ it is possible to determine $\langle I_c \rangle$ and thus $\langle I_f \rangle$ and $|g_{1,f}(\tau)|$. However, for comparisons with solutions of the correlation diffusion equation it is not necessary to make this separation, it is only necessary that $g_{1,c}(\tau) \approx 1$ for the temporal region of interest.

4.3 Experimental Results

4.3.1 Validity of Diffusion Equation for Media with Spatially Varying Brownian Motion

This section compares experimental and theoretical results to verify the validity of the correlation diffusion equation for turbid media with spatially varying dynamical and optical properties. The experiments are performed on a turbid slab which is static and homogeneous except for a spherical region which is dynamic. Dynamic regions with different magnitudes of Brownian motion and different scattering coefficients are considered.

Before discussing the experiment I briefly review the solution to eq. (4.22) for a medium which is homogeneous except for a spherical region (with radius a) characterized by different optical and dynamical properties than the surrounding medium. The spherical region can also be characterized by different optical properties. The analytic solution of the correlation diffusion equation for this system reveals that the measured correlation function outside the sphere can be interpreted as a superposition of the incident correlation plus a term which accounts for the "scattering" of the correlation

from the sphere, i.e.

$$G_1^{out}(\mathbf{r_s}, \mathbf{r_d}, \tau) = \frac{S \exp(i K^{out}(\tau)|\mathbf{r_d} - \mathbf{r_s}|)}{4\pi D_\gamma |\mathbf{r_d} - \mathbf{r_s}|} + \sum_{l=0}^{\infty} A_l h_l^{(1)}(K^{out}(\tau)\mathbf{r_d}) Y_l^0(\theta, \phi) \ . \quad (4.43)$$

Here, $h_l^{(1)}$ are Hankel functions of the first kind and $Y_l^0(\theta, \phi)$ are spherical harmonics. The sphere is centered on the origin, and the source is placed on the z-axis to exploit azimuthal symmetry. The coefficient A_l is the scattering amplitude of the lth partial wave and is found by matching the appropriate boundary conditions on the surface of the sphere. The boundary conditions are similar to that for the photon diffusion equation discussed in section 2.5. Specifically, the correlation must be continuous across the boundary as well as the net flux normal to the boundary, i.e. $G_1^{out}(a, \tau) = G_1^{in}(a, \tau)$ and $-D_\gamma^{out}\hat{r} \cdot \nabla G_1^{out}(\mathbf{r}, \tau)|_{r=a} = -D_\gamma^{in}\hat{r} \cdot \nabla G_1^{in}(\mathbf{r}, \tau)|_{r=a}$ on the surface of the sphere. $G_1^{in}(\mathbf{r}, \tau)$ is the correlation function inside the spherical object and $\hat{r}$ is the normal vector to the sphere. Applying these boundary conditions, we find

$$A_l = \frac{-iv S K^{out}}{D_\gamma^{out}} h_l^{(1)}(K^{out} z_s) Y_l^{0*}(\pi, 0) \left[\frac{D_\gamma^{out} x j_l'(x) j_l(y) - D_\gamma^{in} y j_l(x) j_l'(y)}{D_\gamma^{out} x h_l^{(1)\prime}(x) j_l(y) - D_\gamma^{in} y h_l^{(1)}(x) j_l'(y)} \right] , (4.44)$$

where j_l are the spherical Bessel functions of the first kind, $x = K^{out}a$, $y = K^{in}a$, a is the radius of the sphere, $\mathbf{r_s}$ is the position of the source, and j_l' and $h_l^{(1)\prime}$ are the first derivatives of the functions j_l and $h_l^{(1)}$ with respect to the argument. This solution has been discussed in detail for DPDW's in section 2.5 [29, 30]. By viewing the perturbation of temporal correlation as a scattering process, simple algorithms adapted from scattering theory can be applied to reconstruct images of spatially varying dynamics in turbid media.

I demonstrate the scattering of temporal correlation by a dynamical inhomogeneity in an experiment shown in fig. 4.6. In this experiment, the temporal intensity correlation function is measured in remission from a semi-infinite, highly-scattering, solid slab of TiO_2 suspended in resin ($D_B = 0$). The slab contains a spherical cavity filled with a turbid, fluctuating suspension of 0.296 μm polystyrene balls ($D_B = 1.5 \times 10^{-8}$ cm^{2}s^{-1}). The measured temporal intensity correlation function, $g_2(\tau)$, for three different source detector separations is presented in fig. 4.7. $g_2(\tau)$ is plotted for the system with no
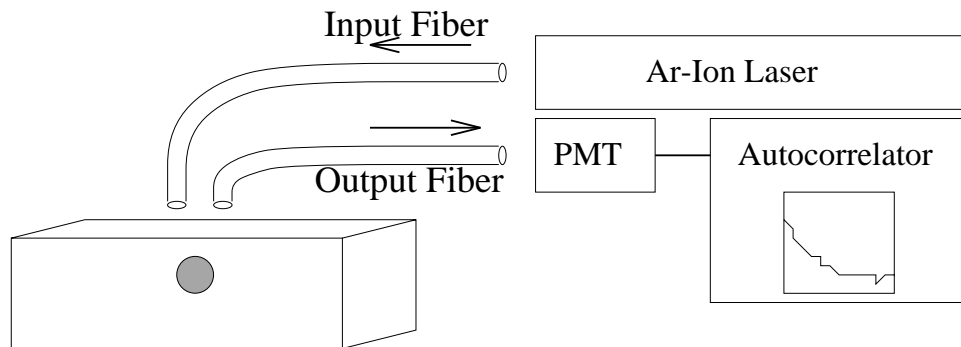
Figure 4.6: The 514 nm line from an argon ion laser (operated at 2.0 W with an etalon) is coupled into a multi-mode fiber optic cable and delivered to the surface of a solid slab of TiO_2 suspended in resin. The slab has dimensions of 15x15x8 cm. A spherical cavity with a diameter of 2.5 cm is located 1.8 cm below the center of the upper surface. The cavity is filled with a 0.2% suspension of 0.296 μm diameter polystyrene spheres at 25 °C resulting in $\mu'_s = 6.67$ cm^{-1}, $\mu_a = 0.002$ cm^{-1}, and $D_B = 1.5 \times 10^{-8}$ cm^{2}s^{-1}. For the solid, $\mu'_s = 4.55$ cm^{-1} and $\mu_a = 0.002$ cm^{-1}. A single-mode fiber collects light at a known position and delivers it to a photo-multiplier tube (PMT), whose output enters a digital autocorrelator to obtain the temporal intensity correlation function. The temporal intensity correlation function is related to the temporal field correlation function by the Siegert relation [100, 48, 50]. The fibers can be moved to any position on the sample surface.
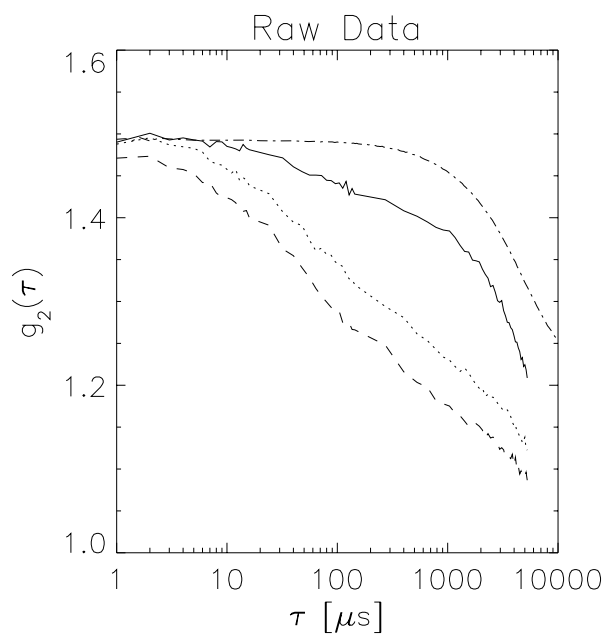
Figure 4.7: Experimental measurements of the temporal intensity autocorrelation function for three different source-detector pairs with a colloid present and one source-detector position without the colloid. The dot-dashed line illustrates the decay of the correlation function due to ensemble averaging (i.e. no colloid is present). This decay is independent of source-detector position. The dashed, dotted, and solid lines correspond to $g_2(\tau)$ measured with a colloid in the cavity and source-detector positions respectively at 1, 2, and 3 as indicated in fig. 4.8.

Brownian motion (i.e. no colloid is present) to illustrate the time scale introduced by ensemble averaging. From the raw data we see that $\beta \approx 0.5$, as expected, since we are using a single-mode fiber that propagates the two orthogonal polarizations. We also observe the short time decay of the correlation function due to Brownian motion and the long time decay due to ensemble averaging. The decay due to ensemble averaging is significant for $\tau > 300$ μs and is not dependent on source-detector position or separation.

Fig. 4.8 plots the decay of the normalized temporal field correlation function, $g_1(\tau)$, obtained from $g_2(\tau)$ and compares these results to theoretical predictions based on eq. (4.43). The expected trend is observed. When the source and detector are closer to the dynamical region, there is more decay in the correlation function and the rate of decay is greater. Here the largest fraction of detected photons have sampled the dynamical region and on average have had more scattering events in the dynamical region. The agreement between experiment and theory is NOT good. In order to get good agreement the Brownian diffusion coefficient must be reduced by a factor of 3 to 4. For the theoretical results presented in fig. 4.8, $D_B = 3.77 \times 10^{-9}$ cm^{2}s^{-1} which is a factor of ~ 4 smaller than the expected $D_B = 1.5 \times 10^{-8}$ cm^{2}s^{-1}. The cause of this discrepancy is discussed below.

Although quantitative agreement is not observed, qualitative agreement is observed. Correlation functions were measured for different reduced scattering coefficients and Brownian diffusion coefficients for the dynamical region. Fig. 4.9 plots the measured correlation functions for different μ_s' compared with theory. Three different concentrations of 0.813 μm diameter polystyrene microspheres where used to obtain reduced scattering coefficients of 3.5, 4.5, and 9.0 cm^{-1} for the dynamical region. The rest of the system is the same as the previous experiment (see fig. 4.6). Using the Brownian diffusion coefficient as a free parameter to fit the theory to experiment, good agreement was obtained. In all cases the Brownian diffusion coefficient had to be reduced by a factor of ~ 3. For 0.813 μm diameter polystyrene microspheres the expected D_B is 5.46×10^{-9} cm^{2}s^{-1}. For μ_s'=3.5, 4.5, and 9.0 cm^{-1} the fits for D_B where
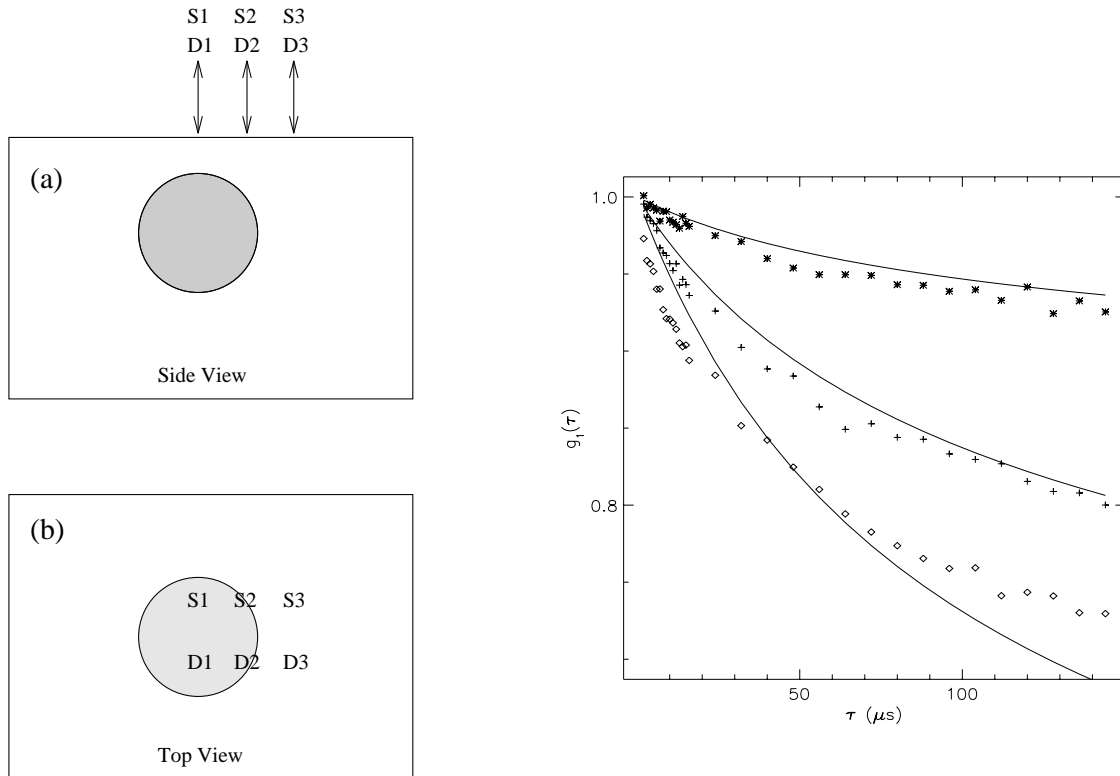
Figure 4.8: Experimental measurements of the normalized temporal field autocorrelation function for three different source-detector pairs are compared with theory. The geometry is illustrated in (a) and (b). With respect to an x-y coordinate system whose origin lies directly above the center of the spherical cavity, the source-detector axis was aligned parallel to the y-axis with the source at y=1.0 cm and the detector at y=-0.75 cm. Keeping the source-detector separation fixed at 1.75 cm, measurements were made at x=0.0 cm, 1.0 cm, and 2.0 cm, and are indicated by the ◇'s, +'s, and ∗'s respectively. The uncertainty for these measurements is 3% and arises from uncertainty in the position of the source and detector. The solid line was calculated using the known experimental parameters with D_B as a free parameter (see fig. 4.6). Note larger and more rapid decays are observed when the source and detector are nearest the dynamic sphere.

2.21×10^{-9}, 2.14×10^{-9}, and 1.78×10^{-9} cm^{2}s^{-1} respectively.

Correlation functions for different Brownian diffusion coefficients are plotted in fig. 4.10. Different D_B were obtained by using monodisperse polystyrene microspheres with diameters of 0.137 μm, 0.300 μm, and 0.813 μm. The concentrations were varied to keep μ'_s=4.5 cm^{-1}. Once again good agreement between experiment and theory was observed by using a smaller D_B in the theory. The relative values for the fitted D_B agree with that of the experimental D_B. The expected values of D_B were 3.28×10^{-8}, 1.50×10^{-8}, and 5.46×10^{-9} cm^{2}s^{-1} respectively for the 0.137 μm, 0.300 μm, and 0.813 μm diameter polyballs. The fitted values for D_B were 1.49×10^{-8}, 8.21×10^{-9}, and 2.71×10^{-9} cm^{2}s^{-1}.

I believe the observed disagreement in the Brownian diffusion coefficient results from mismatches in the indices of refraction at the resin/air and resin/colloid interfaces. In an early analysis [94] the semi-infinite boundary condition was solved incorrectly, but fortuitously resulted in better agreement. In that case [94], the point source was not placed a distance of $l^* = 1/\mu'_s$ away from the collimated source along the source axis as in the usual treatment of a collimated source [76], but rather at the collimated source position. Furthermore, the image source (to satisfy the extrapolated boundary condition for index mismatched media) was positioned as if the real source had been extended into the medium. This treatment resulted in quantitative agreement between theory and experiment.

The high sensitivity to the treatment of the semi-infinite boundary conditions renders this experimental setup inappropriate for rigorously validating the correlation diffusion equation for systems with spatially varying dynamical and optical properties. In the next section I compare the theory with Monte Carlo results for infinite media with spherical inhomogeneities and obtain quantitative agreement. The agreement supports the view that correlation "scatters" from spatial variations of the particle diffusion coefficient $(D_B(\mathbf{r}))$, the absorption $(\mu_a(\mathbf{r}))$, and the reduced scattering coefficient $(\mu'_s(\mathbf{r}))$.
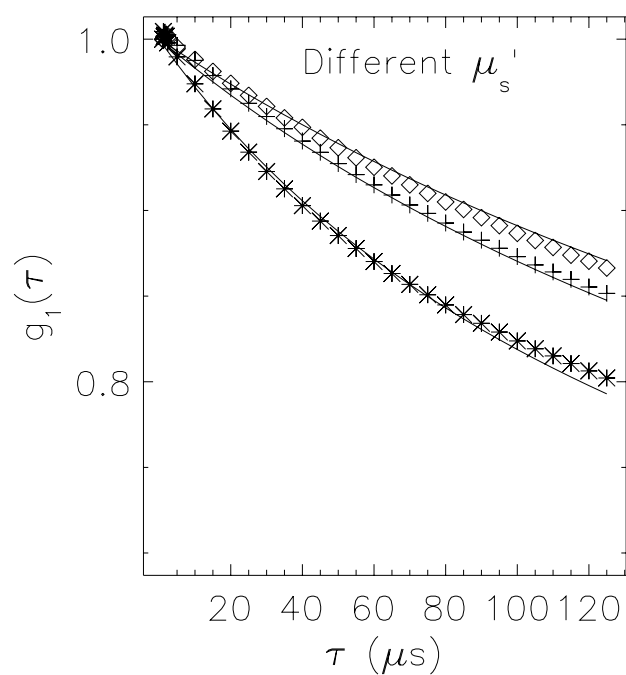
Figure 4.9: Experimental measurements of the normalized field correlation function for a dynamical region with three different μ'_s are plotted. The source and detector were separated by 1.5 cm and centered over the position of the sphere. The ◇'s, +'s, and *'s correspond to $\mu'_s=$ 3.5, 4.5, and 9.0 cm^{-1} respectively. The solid line was calculated using the known experimental parameters with D_B as a free parameter.
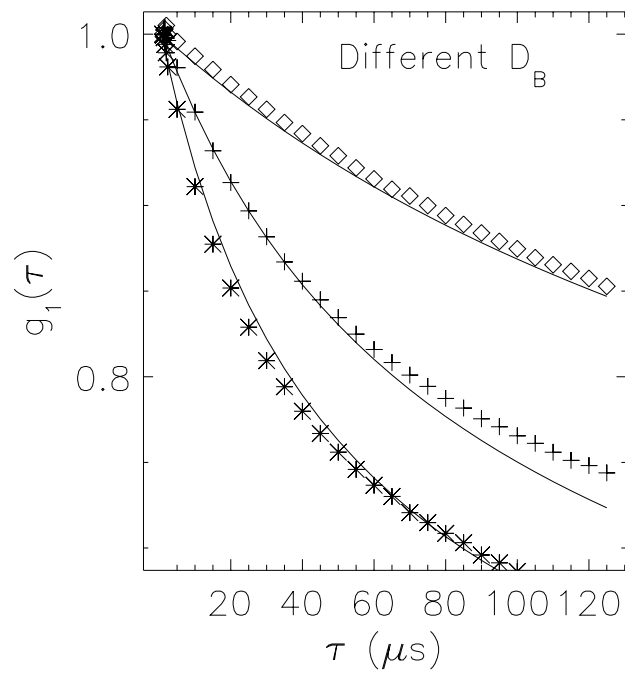
Figure 4.10: Experimental measurements of the normalized field correlation function for a dynamical region with three different D_B are plotted. The source and detector were separated by 1.5 cm and centered over the position of the sphere. The ◇'s, +'s, and *'s correspond to $a=$ 0.813, 0.300, and 0.137 μm respectively. The solid line was calculated using the known experimental parameters with D_B as a free parameter.

4.3.2   Imaging Media with Spatially Varying Brownian Motion

Since the perturbation of correlation by inhomogeneities can be viewed as a scattering process, one can readily envision the application of tomographic algorithms for the reconstruction of images of spatially varying dynamics [13]. I have investigated this possibility. I use an inversion algorithm, one of several possible schemes [13, 113], which is based on a solution to the correlation diffusion equation, eq. (4.22), generalized to include spatially varying dynamics, $D_B(\mathbf{r}) = D_{B,o} + \delta D_B(\mathbf{r})$, absorption, $\mu_a(\mathbf{r}) = \mu_{a,o} + \delta\mu_a(\mathbf{r})$, and scattering, $\mu'_s(\mathbf{r}) = \mu'_{s,o} + \delta\mu'_s(\mathbf{r})$ and $D_\gamma(\mathbf{r}) = D_{\gamma,o} + \delta D_\gamma(\mathbf{r})$. $D_{B,o}$, $\mu'_{s,o}$, and $\mu_{a,o}$ are the spatially uniform background characteristics. $\delta\mu_a(\mathbf{r})$ is the spatial variation in the absorption coefficient, $\delta\mu'_s(\mathbf{r})$ is the spatial variation in the reduced scattering coefficient, $\delta D_\gamma(\mathbf{r})$ is the spatial variation in the photon diffusion coefficient, and $\delta D_B(\mathbf{r})$ represents the spatial variation in the particle diffusion coefficient relative to the background value.

The correlation diffuse equation with spatially varying optical and dynamical properties is

$$\nabla^2 G_1(\mathbf{r_s}, \mathbf{r}, \tau) - \frac{v\mu_{a,o}}{D_{\gamma,o}} G_1(\mathbf{r_s}, \mathbf{r}, \tau) - \frac{2v\mu'_s k_o^2 D_{B,o}\tau}{D_{\gamma,o}} G_1(\mathbf{r_s}, \mathbf{r}, \tau) =$$

$$-\frac{v}{D_\gamma(\mathbf{r})} S_o \delta(\mathbf{r_s} - \mathbf{r}) + \frac{1}{\mu'_{s,o}} \nabla\delta\mu'_s(\mathbf{r}) \cdot \nabla G_1(\mathbf{r_s}, \mathbf{r}, \tau) + \frac{v\delta\mu_a(\mathbf{r})}{D_{\gamma,o}} G_1(\mathbf{r_s}, \mathbf{r}, \tau)$$

$$+\frac{2v\mu'_s k_o^2 \delta D_B(\mathbf{r})\tau}{D_{\gamma,o}} G_1(\mathbf{r_s}, \mathbf{r}, \tau) + 3\mu_{a,o}\delta\mu'_s G_1(\mathbf{r_s}, \mathbf{r}, \tau) \ . \tag{4.45}$$

This equation can be solved using the first Born approximation as is described in section 2.5.5. We can also solve this equation using the Rytov approximation [113]. Within the Rytov approximation we assume that $G_1(\mathbf{r_s}, \mathbf{r}, \tau) = G_{1,o}(\mathbf{r_s}, \mathbf{r}, \tau)$ $\exp\left(\Phi_s(\mathbf{r_s}, \mathbf{r}, \tau)\right)$. Following the procedure described by Kak and Slaney [113] we obtain an integral equation relating $\Phi_s(\mathbf{r_s}, \mathbf{r}, \tau)$ to the spatial variation of the dynamical and optical properties, i.e.

$$\Phi_s(\mathbf{r_s}, \mathbf{r_d}, \tau) = -\frac{1}{G_1^o(\mathbf{r_s}, \mathbf{r_d}, \tau)} \int \mathrm{d}^3 r' \left[\frac{2v\mu'_s k_o^2 \tau \delta D_B(\mathbf{r'})}{D_{\gamma,o}} H(\mathbf{r'}, \mathbf{r_d}, \tau) G_1^o(\mathbf{r_s}, \mathbf{r'}, \tau) \right.$$

$$\left. +\frac{v\delta\mu_a(\mathbf{r})}{D_{\gamma,o}} H(\mathbf{r'}, \mathbf{r_d}, \tau) G_1^o(\mathbf{r_s}, \mathbf{r'}, \tau) + \frac{\delta D_\gamma(\mathbf{r})}{D_{\gamma,o}} \nabla G_1^T(\mathbf{r}, \hat{\Omega}, \tau)_1^{(0)}(\mathbf{r_s}, \mathbf{r}) \cdot \nabla H(\mathbf{r}, \mathbf{r_d}) \right] \tag{4.46}$$
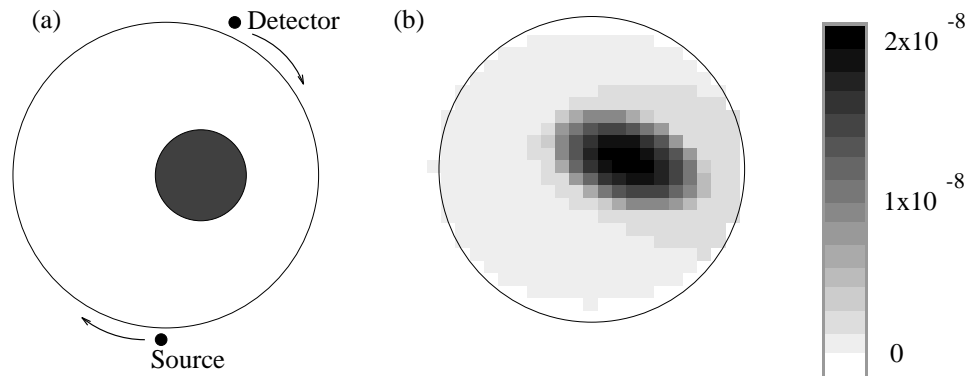
Figure 4.11: An image reconstructed from experimental measurements of the scattered correlation function is shown in (b). The system was a 4.6 cm diameter cylinder with l^*=0.25 cm, μ_a=0.002 cm^{-1}, and D_B=0 (see illustruction in (a)). A 1.3 cm diameter spherical cavity was centered at x=0.7 cm, y=0, and z=0 and filled with a colloid with l^*=0.25 cm, μ_a=0.002 cm^{-1}, and D_B=1.5x10^{-8}cm^{2}s^{-1}. A slice of the image at z=0 cm is presented in (b). The values of the reconstructed particle diffusion coefficients are indicated by the legend in units of cm^{2}s^{-1}.

Here, $H(\mathbf{r}', \mathbf{r_d}, \tau)$ is the Green's function for the homogeneous correlation diffusion equation, $\delta\mu_a(\mathbf{r})$ is the spatial variation in the absorption coefficient, $\delta D_\gamma(\mathbf{r})$ is the spatial variation in the photon diffusion coefficient, and $\delta D_B(\mathbf{r})$ represents the spatial variation in the particle diffusion coefficient relative to the background value. The position of the source (detector) is $\mathbf{r_s}$ ($\mathbf{r_d}$).

There are many techniques that can be employed to invert eq. (4.46) [13, 113]. All the methods are based on discretizing the integral equation and using measurements of $\Phi_s(\mathbf{r_s}, \mathbf{r_d})$ with several different source-detector pairs to solve the coupled set of linear equations (see section 2.5.5). I use the Simultaneous Iterative Reconstruction Technique [113] to solve the coupled equations.

To demonstrate that the correlation diffusion equation can be used as the basis for a tomographic reconstruction algorithm, I took several measurements on a solid, highly-scattering sample that contained a spherical, dynamical region. The system was

a solid cylinder of TiO_2 suspended in resin. The cylinder was homogeneous except for a 1.3 cm diameter spherical cavity which was filled with an aqueous suspension of 0.296 μm polystyrene balls ($D_B = 1.5 \times 10^{-8}$ cm^{2}s^{-1}) and centered at z=0 (the z-axis is the axis of the cylinder). The optical properties of the colloid matched that of the solid so that we are only imaging variations in the dynamical properties. Measurements were made every 30° at the surface of the cylinder for z=0, 1, and 2 cm, with source-detector angular separations of 30° and 170° and correlation times of τ= 15, 25, 35, 45, 55, 65, 75, and 85 μs. Except where the measurements were made, a highly reflective coating was applied to the surface so that the cylindrical medium could be treated as infinite. This approximation has been discussed by Haskell *et al.* [76] and its validity permits us to obtain accurate reconstructions of the dynamical properties.

The image of $D_B(\mathbf{r})$ in fig. 4.11 was reconstructed from ~ 600 measurements of the scattered correlation function, $\Phi_s(\mathbf{r_s}, \mathbf{r_d}, \tau)$, using 400 iterations of the Simultaneous Iterative Reconstruction Technique [113]. The z=0 slice of the image is shown in fig. 4.11b. From this image the center (in the x-y plane) of the dynamic region and the magnitude of the particle diffusion coefficient are determined. The center of the object in the image is within 2 mm of the actual center of the dynamic sphere. This discrepancy scales with the uncertainty in the position of the source and detector. The sphere diameter (~ 1.3 cm) and particle diffusion coefficient ($\sim 1.8 \times 10^{-8}$ cm^{2}s^{-1}) obtained from the imaging procedure also agree reasonably well with experimentally known parameters (1.3 cm and 1.5×10^{-8} cm^{2}s^{-1}).

4.3.3   Validity of Diffusion Equation for Media with Spatially Varying Flow Properties

The experiments described thus far demonstrate the diffusion and scattering of correlation in turbid samples where the dynamics are governed by Brownian motion. The correlation diffusion equation can be modified to account for other dynamical processes. In the cases of random flow and shear flow the correlation diffusion equation

becomes

$$\left(D_\gamma \nabla^2 - v\mu_a - 2v\mu'_s D_B k_o^2 \tau - \frac{1}{3}v\mu'_s \left\langle \Delta V^2 \right\rangle k_o^2 \tau^2 - \frac{1}{15}v\mu'^{-1}_s \Gamma^2_{eff} k_o^2 \tau^2 \right) G_1(\mathbf{r}, \tau) = -vS(\mathbf{r}).$$
$$(4.47)$$

The fourth and fifth terms on the left-hand side of eq. (4.47) arise from random and shear flows respectively. $\left\langle \Delta V^2 \right\rangle$ is the second moment of the particle speed distribution (assuming the velocity distribution is isotropic and Gaussian)[103, 46], and Γ_{eff} is the effective shear rate [104]. Notice that the "dynamical absorption" for flow in eq. (4.47) increases as τ^2 (compared to the τ increase for Brownian motion) because particles in flow fields travel ballistically; also D_B, $\left\langle \Delta V^2 \right\rangle$, and Γ_{eff} appear separately because the different dynamical processes are uncorrelated. The form of the "dynamical absorption" term for random flow is related to that for Brownian motion. Both are of the form $\frac{1}{3}v\mu'_s \left\langle \Delta r^2(\tau) \right\rangle$, where $\left\langle \Delta r^2(\tau) \right\rangle$ is the mean square displacement of a scattering particle. For Brownian motion $\left\langle \Delta r^2(\tau) \right\rangle = 6D_B\tau$, and for random flow $\left\langle \Delta r^2(\tau) \right\rangle = \left\langle \Delta V^2 \right\rangle \tau^2$. The derivation of the "dynamical absorption" term for shear flow is more complex and the reader is referred to Wu *et al.* [104] for a complete discussion.

Flow in turbid media is an interesting problem that has received some attention. In these measurements experimenters typically determine a correlation function that may be a compound of many decays representing a weighted average of flow within the sample. For example, Bonner and Nossal have developed an approach for measuring random blood flow in homogeneous tissue [46], Wu *et al.* have applied DWS to study uniform shear flow [104], and Bicout and co-workers have applied DWS to study inhomogeneous flow and turbulence [114, 115, 116, 117]. In all cases, *a priori* knowledge of the flow is used in the analyses. The application of correlation diffusion imaging will further clarify information about heterogeneous flows in turbid media.

I conducted experiments to examine the correlation signal arising from a solid highly scattering medium with a single cylindrical vein containing a highly scattering liquid under Poiseuille flow. The experimental system is depicted in fig. 4.12. In this experiment, the correlation function is measured in remission from a semi-infinite,
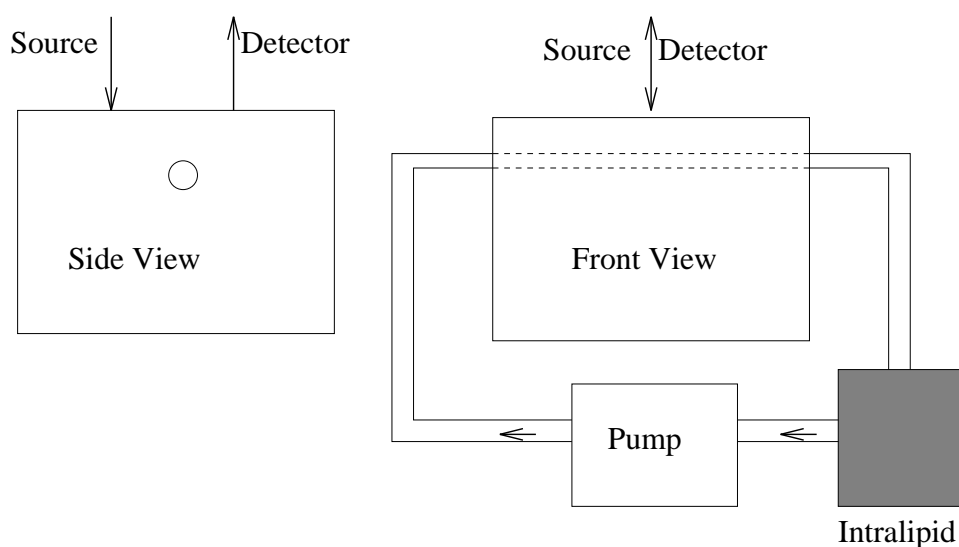
Figure 4.12: The experimental system is the same as described in fig. 4.6 except that the TiO_2 slab now has a 6 mm diameter cylindrical cavity instead of a spherical cavity. The cylindrical cavity is centered 13 mm below the surface of the slab and 0.5% Intralipid is pumped through the cavity at flow speeds of 0.442 cm s^{-1}, 0.884 cm s^{-1}, and 1.77 cm s^{-1}. For the solid, $\mu'_s = 4.0$ cm^{-1} and $\mu_a = 0.002$ cm^{-1}. For the Intralipid, the optical properties are assumed to be the same as the TiO_2. The correlation function is measured with the source and detector separated by 2.0 cm, i.e. the source is 1.0 cm to the left of the vein and the detector is 1.0 cm to the right.
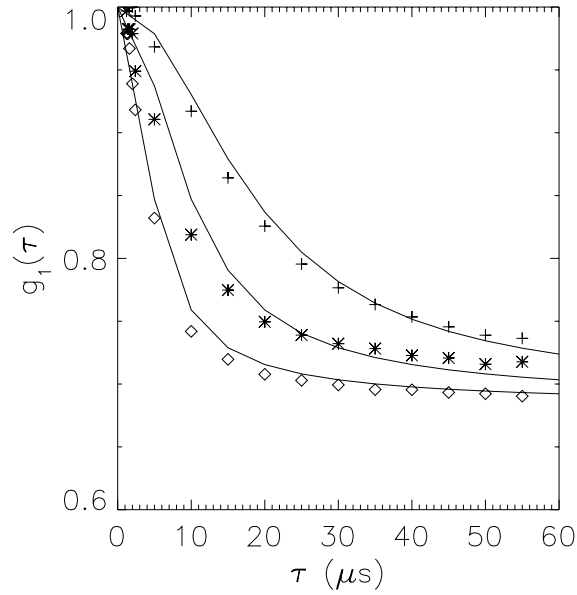
Figure 4.13: Experimental measurements of the normalized temporal field correlation function for three different flow speeds are compared with theory. Measurements for flow speeds of 0.442 cm s^{-1}, 0.884 cm s^{-1}, and 1.77 cm s^{-1} are indicated respectively by the +'s, *'s, and ⋄'s. The solid lines are calculated using the experimental parameters given in fig. 4.12 and effective shear rates of 3.0 s^{-1}, 6.0 s^{-1}, and 12.0 s^{-1}.

highly-scattering, solid slab of TiO$_2$ suspended in resin ($\Gamma_{eff} = 0$). A 0.5% solution of Intralipid [71] is pumped through the cylindrical vein in the slab with pump speeds of 0.442 cm s^{-1}, 0.884 cm s^{-1}, and 1.77 cm s^{-1}. The experimental results are shown by the symbols in fig. 4.13.

Measurements of the normalized temporal field correlation function were compared with the exact solution of correlation scattering from cylindrical inhomogeneities. The derivation of the analytic solution for a cylinder is similar to that for a sphere. Once again, the correlation is a superposition of the incident and scattered correlation, i.e. $G_1^{out} = G_1^{o} + G_1^{scatt}$. For a cylinder of infinite length, the solution for the scattered wave in cylindrical coordinates is [118]

$$G_1^{scatt}(r, \theta, z) = -\frac{vS}{2\pi^2 D_\gamma} \sum_{n=1}^{\infty} \int_0^{\infty} \mathrm{d}p \cos(n\theta) \cos(pz)$$

$$\times K_n(\sqrt{p^2 - (K^{out})^2}\ r)K_n(\sqrt{p^2 - (K^{out})^2}\ r_s)$$
$$\times \left[\frac{D_\gamma^{out}x I_n'(x)I_n(y) - D_\gamma^{in}y I_n(x)I_n'(y)}{D_\gamma^{out}x K_n\prime(x)I_n(y) - D_\gamma^{in}y K_n(x)I_n\prime(y)}\right]\ , \tag{4.48}$$

where I_n and K_n are modified Bessel functions, $x = \sqrt{p^2 - (K^{out})^2}\ a$, $y = \sqrt{p^2 - (K^{in})^2}\ a$, and a is the radius of the cylinder. The solution has been simplified by taking the z-axis as the axis of the cylinder and assuming that the source is at $z = 0$ and $\theta = 0°$.

The comparison between experiment (symbols) and theory (solid lines) shown in fig. 4.13 indicates a good agreement. The parameters used in the calculation, except for Γ_{eff}, were the known parameters. The effective shear rate, Γ_{eff}, was determined by fitting the analytic solution to the data with the constraint that Γ_{eff} had to scale linearly with the flow speed. The best fit to the data indicates that Γ_{eff} is approximately 6.8 cm^{-1} times the flow speed. Since the shear rate is given by the change in speed per unit length in the direction perpendicular to the flow, one might expect that the effective shear rate would be the flow speed divided by the radius of the vein. This simple calculation gives an effective shear rate that is a factor of two smaller than the measured Γ_{eff}. This difference is not yet understood, but could result from the mismatches in optical indices of refraction and sensitivity to the semi-infinite boundary condition.

4.4   Monte Carlo Simulations

This section presents the results of various Monte Carlo simulations of correlation diffusion. I used the results from Monte Carlo simulations to check the accuracy of the correlation diffusion equation when the accuracy of my experimental results was questionable or I did not have the experimental data. In many cases these simulations provide a signal-to-noise ratio that is difficult to achieve in the laboratory and therefore permit a more accurate test of the validity of the correlation diffusion theory.

I first present simulation results for an infinite, homogeneous system compared

with correlation diffusion theory. This comparison illustrates the behavior of the correlation function as different parameters are varied. Good agreement with diffusion theory is observed. I then present results for a system which is infinite, static, and homogeneous except for a spherical dynamic region. This system avoids the shortcomings of the experimental system used in the previous section. Results are compiled for a wide range of parameters and compared with correlation diffusion theory. The agreement is good indicating the robustness of the theory. I then present simulations for a two-component system with spatially uniform random flow in a spatially uniform static medium. This system models a capillary network in tissue. The comparison with correlation diffusion theory demonstrates that the homogeneous solution can be used as long as the dynamical term is weighted by

$$
\frac{\mu_s'(\text{random flow component})}{\mu_s'(\text{random flow component}) + \mu_s'(\text{static component})} \ . \tag{4.49}
$$

The Monte Carlo simulations for obtaining electric field temporal autocorrelation functions is described in appendix 6.2.2. Briefly, the approach is to histogram the accumulated momentum transfer of photons scattered from moving particles as they propagate through a system with spatially varying dynamics. That is, scattering events in a static medium do not contribute to the accumulated momentum transfer while scattering events in a dynamic medium do contribute. The contribution is proportional to the magnitude of the dynamics. In the simulation the momentum transfer is accumulated as a dimensionless variable that scales with k_o^2. The histogram, when normalized, is just the momentum transfer probability distribution $P(Y)$. The correlation function can then be calculated with [119, 120]

$$
g_1(\tau) = \int_0^\infty dY\, P(Y) \exp\left(-\frac{1}{3} Y k_o^2 \left\langle \Delta r^2(\tau) \right\rangle\right) \ . \tag{4.50}
$$

$P(Y)$ is determined from the Monte Carlo simulation, k_o^2 is the wavenumber of light in the medium, and $\left\langle \Delta r^2(\tau) \right\rangle$ is determined by the dynamics of the system.
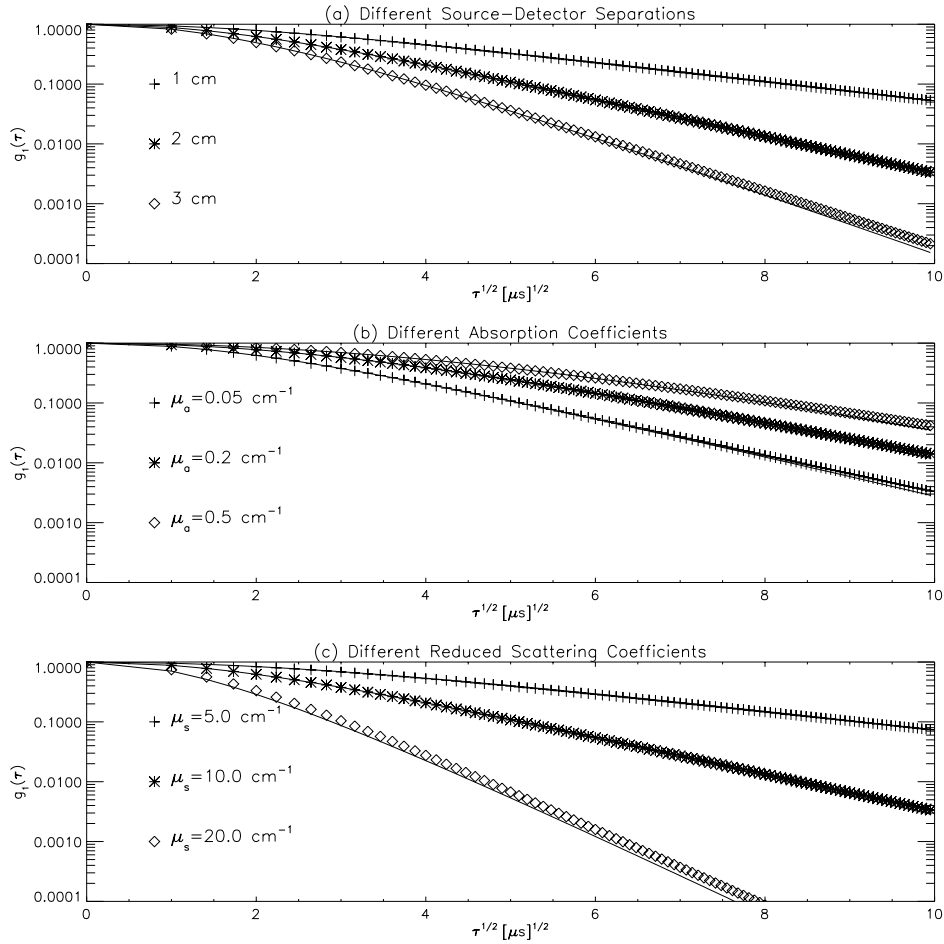
Figure 4.14: Monte Carlo simulations for correlation diffusion in a homogeneous medium are compared with theory for different (a) source-detector separations, (b) absorption coefficients, and (c) reduced scattering coefficients. Unless otherwise stated, the source-detector separation is 2.0 cm, $\mu_s'=10.0$ cm^{-1}, $\mu_a=0.05$ cm^{-1}, and $D_B = 1.0 \ 10^{-8}$ cm^{2}s^{-1}. The Monte Carlo results are given by the symbols. The solid lines are calculated from diffusion theory.

4.4.1   Homogeneous Media with Brownian Motion

Comparisons of eq. (4.13) with experimental measurements of absorption-free media has been made by Pine *et al.* [106]. Good agreement is found except in regimes where the photon diffusion approximation breaks down. Here, I compare solutions of the correlation diffusion equation with photon absorption to Monte Carlo simulations. In this case, the solution is

$$G_1(\mathbf{r}, \tau) = \frac{S \exp\left(-\sqrt{3\mu_a\mu'_s + 6\mu'^2_s D_B k_o^2 \tau}\; |\mathbf{r} - \mathbf{r_s}|\right)}{4\pi D_\gamma |\mathbf{r} - \mathbf{r_s}|} \; . \tag{4.51}$$

At early correlation times the behavior is governed by photon absorption and at later times it is governed by dynamical processes. The transition time is given by $\tau_c = \mu_a/(2\mu'_s D_B k_o^2)$. At shorter τ the correlation function will plateau while at longer τ it will decay exponentially as the square-root of τ with the same rate as if there were no photon absorption.

Fig. 4.14a plots the Monte Carlo results for different source-detector separations ρ. The optical and dynamical properties are held constant at $\mu'_s = 10.0$ cm^{-1}, $\mu_a = 0.05$ cm^{-1}, and $D_B = 1\mathrm{x}10^{-8}$ cm^{2}s^{-1}. The decay rate of $g_1(\tau)$ increases linearly with ρ, as expected. Next, we see the plateau at early τ and that the transition time is independent of ρ. Finally, $g_1(\tau)$ calculated using correlation diffusion theory for the different source-detector separations is given by the solid lines. In all cases good agreement is observed.

Results for varying μ_a and μ'_s while keeping the source-detector separation fixed are given in fig. 4.14b and fig. 4.14c respectively. In fig. 4.14b we see that τ_c increases as the absorption coefficient is increased while the decay rate at $\tau > \tau_c$ is not changed. In fig. 4.14c we see that increasing the reduced scattering coefficient increases the decay rate of the correlation function and decreases τ_c. In all cases, good agreement with diffusion theory is observed.

Fig. 4.15 plots the same correlation functions plotted in fig. 4.14 for different source-detector separations, but the abscissa is extended from 100 μs to 400 μs. At these longer correlation times the correlation diffusion equation is expected to break down
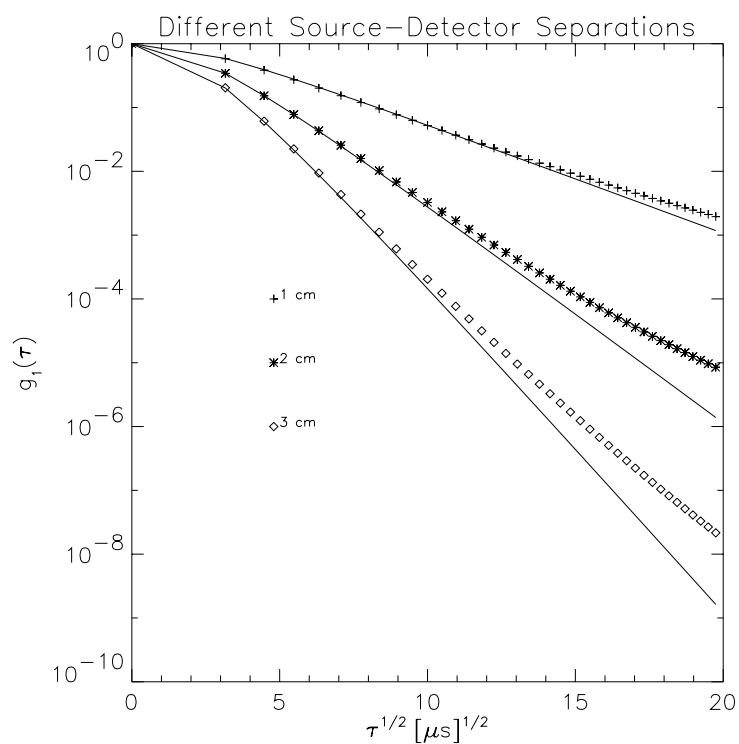
Figure 4.15: Monte Carlo simulations for correlation diffusion in a homogeneous medium are compared with theory for different source-detector separations. Monte Carlo results are given by the symbols. The solid lines are calculated from diffusion theory.

because of the approximation that $k_o^2 \langle \Delta r^2(\tau) \rangle \ll 1$. The results in fig. 4.15 indicate that the approximation is not valid when $k_o^2 \langle \Delta r^2(\tau) \rangle \geq 0.1$, that is, when $\tau \geq 225 \mu s$. The magnitude of the deviation depends on the source-detector separation normalized by the photon random walk step length.

The behavior of the deviation is understood. At longer correlation times the decay results from shorter photon path lengths since the longer path lengths have a faster decay rate and no longer provide a significant contribution. For the shorter path lengths the photon diffusion approximation is not valid since the photons are not diffusing. Furthermore, the q average is not appropriate since there have been only a few scattering events, and in order for the photon to reach the detector, the scattering angles must be smaller than average. The smaller than average scattering angles results in the observed slower decay rate of the Monte Carlo simulations relative to diffusion theory.

4.4.2 Media with Spatially Varying Brownian Motion

Here I present Monte Carlo results to check the validity of the correlation diffusion equation for systems with spatially varying dynamical and optical properties. The system is infinite, static, and homogeneous except for a spherical region which is dynamic and may have different optical properties than the background. The homogeneous properties are $\mu_s' = 10.0$ cm^{-1}, $\mu_a = 0.05$ cm^{-1}, and $D_B = 0$ unless otherwise specified. For the sphere, $\mu_s' = 10.0$ cm^{-1}, $\mu_a = 0.05$ cm^{-1}, and $D_B = 1 \times 10^{-8}$ cm^{2}s^{-1} unless otherwise specified. Results are presented for the source-detector positions indicated in fig. 4.16.

Comparison of Monte Carlo results and correlation diffusion theory for a system with spatially varying dynamical properties but uniform optical properties are presented in fig. 4.17. Three different absorption coefficients are considered. In fig. 4.17a, b, and c the absorption coefficients are respectively $\mu_a = 0.02$ cm^{-1}, $\mu_a = 0.05$ cm^{-1}, and $\mu_a = 0.10$ cm^{-1}. For each absorption coefficient, results are presented for the three detector positions. The Monte Carlo results are given by the symbols, and the solid
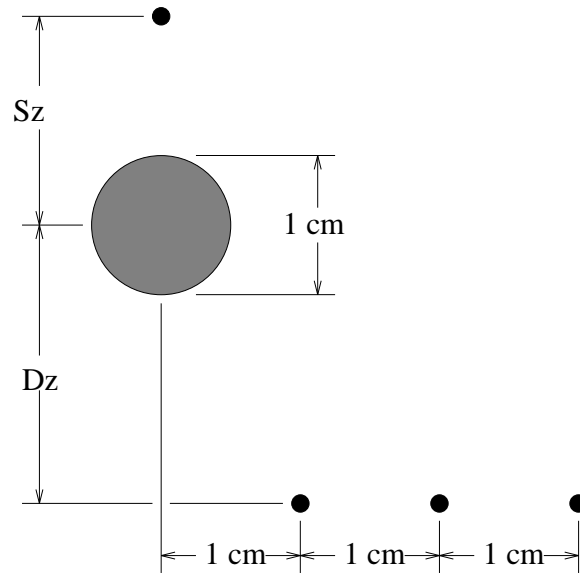
Figure 4.16: An isotropic point source is positioned Sz cm from the center of a spherical inhomogeneity. The sphere has a diameter of 1 cm. Detectors are positioned Dz cm away along the z-axis and displaced off of the z-axis at ρ=1, 2, and 3 cm.

lines indicate the prediction using correlation diffusion theory. The agreement is fairly good. Similar results are found for other Brownian diffusion coefficients; actually the results are the same, except that τ scales inversely with D_B.

The small discrepancies are most likely due to a significant fraction of the fluctuating photons having scattered from the dynamical region only a few times before detection. By fluctuating photons I mean those photons which have sampled the dynamic region as opposed to the static photons which have not seen the dynamic region. The distribution of the total momentum transfer with moving particles for the photons detected at ρ=1.0 cm is plotted in fig. 4.18 for $\mu_a = 0.05$ cm^{-1}. The distribution has a discontinuity at $2k_o$ which is the maximum momentum transfer per scattering event. The diffusion approximation is NOT valid in the regime of a few scattering events. The contribution to $P(Y)$ for $Y < 2$ thus leads to the observed discrepancy. This was checked by noting a correlation between a reduction in the discrepancy with a reduction in the discontinuity for results which are not presented.

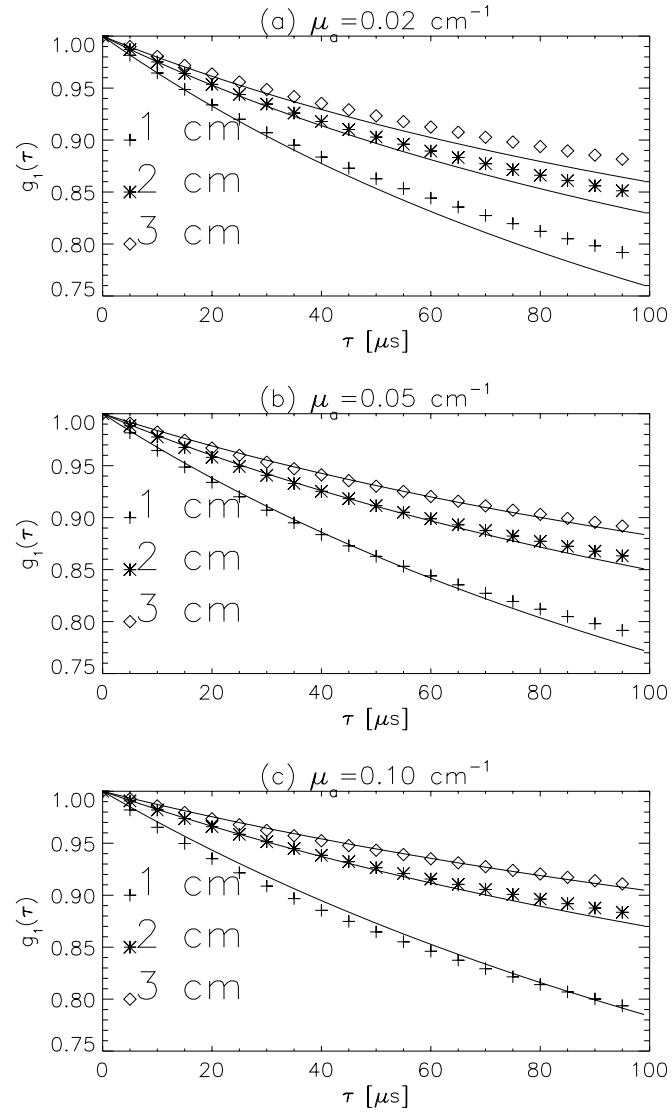In fig. 4.19 I present results for a sphere with different μ_a and D_B than the back-

Figure 4.17: Monte Carlo results for the $g_1(\tau)$ (symbols) are compared with correlation diffusion theory (solid lines) for the system depicted in fig. 4.16. The optical properties are spatially uniform. In (a), (b), and (c) the absorption coefficient is respectively 0.02 cm^{-1}, 0.05 cm^{-1}, and 0.10 cm^{-1}. The ρ position of the detector is indicated in the legend. The source is at Sz=1.0 cm and the detector is at Dz=1.0 cm.
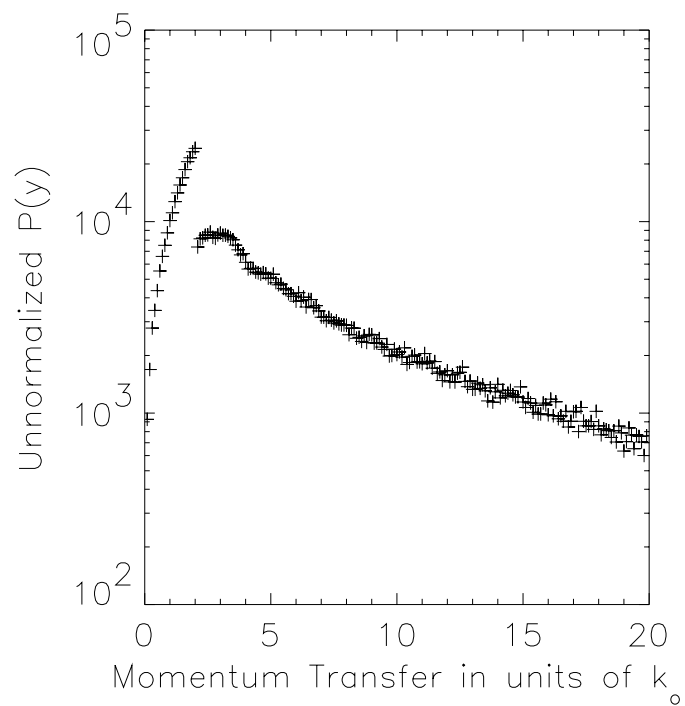
Figure 4.18: Distribution of the total momentum transfer from moving scatterers. The geometry of the system is depicted in fig. 4.16.

ground. For the background $D_B = 0$ while for the sphere $D_B=1 \text{x} 10^{-8}$. For the background $\mu_a = 0.05$ cm^{-1}. For the results presented in fig. 4.19a, b, and c the object absorption coefficient is respectively $\mu_a = 0.02$ cm^{-1}, $\mu_a = 0.05$ cm^{-1}, and $\mu_a = 0.20$ cm^{-1}. When the absorption coefficient of the object is the same as the background then the agreement between Monte Carlo and correlation diffusion is good. However the agreement is not as good when the absorption coefficient of the object is different than the background. This discrepancy results from the breakdown of the photon diffusion equation for systems with spatially varying optical properties. As observed in fig. 4.17 and fig. 4.18 there are many photons which only have a few scattering events in the sphere. The diffusion approximation overestimates the path lengths of these photons in the object. Thus when the absorption coefficient of the object is larger than the background, diffusion theory overestimates the number of absorbed photons, fewer fluctuating photons reach the detector, and the correlation function does not decay as much. For objects with smaller absorption coefficients, diffusion theory overestimates the amount of decay in the correlation function. These are the trends observed in fig. 4.19.

Fig. 4.20 presents results for a sphere with different μ_s' and D_B than the background. For the background $D_B = 0$ while for the sphere $D_B=1 \text{x} 10^{-8}$. For the background $\mu_s' = 10.0$ cm^{-1}. For the results presented in fig. 4.20a, b, and c, the object reduced scattering coefficient is respectively $\mu_s' = 5.0$ cm^{-1}, $\mu_s' = 10.0$ cm^{-1}, and $\mu_s' = 15.0$ cm^{-1}. When the reduced scattering coefficient of the object is the same as the background then the agreement between Monte Carlo and correlation diffusion is good. However the agreement is not as good when the reduced scattering coefficient of the object is different than the background. This discrepancy also results from the breakdown of the photon diffusion equation for systems with spatially varying optical properties.
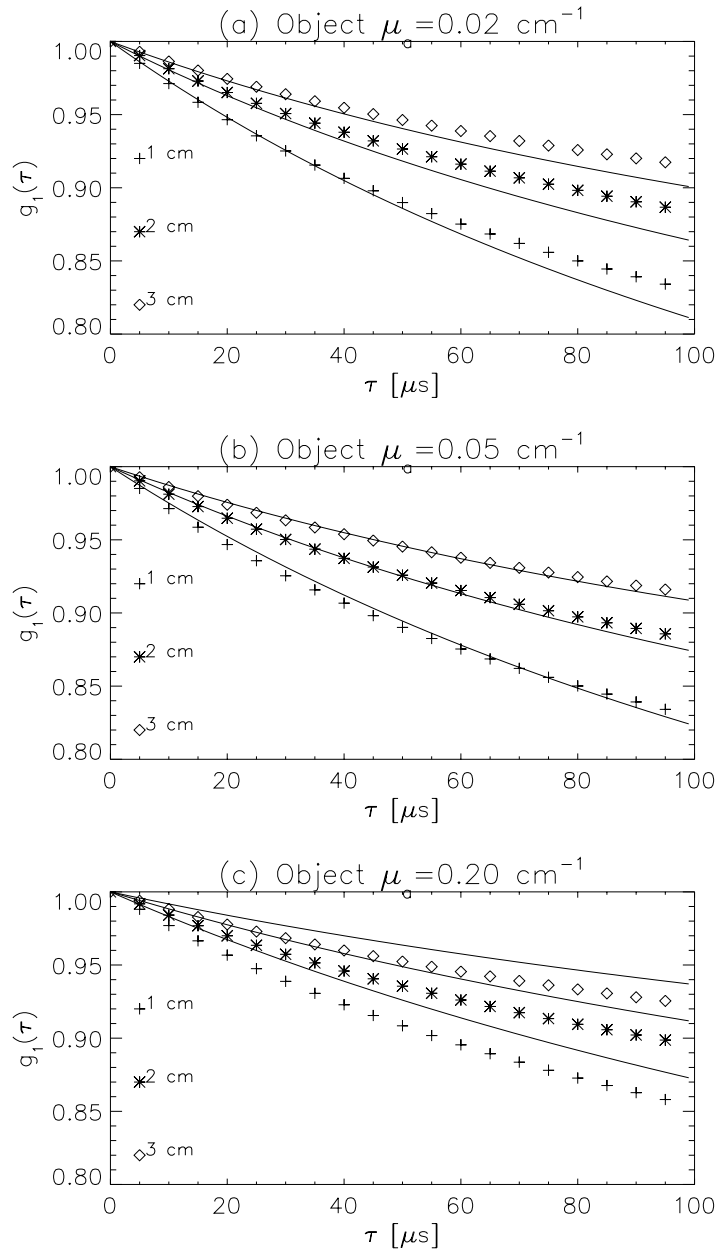
Figure 4.19: Monte Carlo results for $g_1(\tau)$ (symbols) are compared with correlation diffusion theory (lines) for the system depicted in fig. 4.16. In (a), (b), and (c) the object absorption coefficient is respectively 0.02 cm^{-1}, 0.05 cm^{-1}, and 0.20 cm^{-1}. The ρ position of the detector is indicated in the legend. The source is at Sz=1.5 cm and the detector is at Dz=2.0 cm.
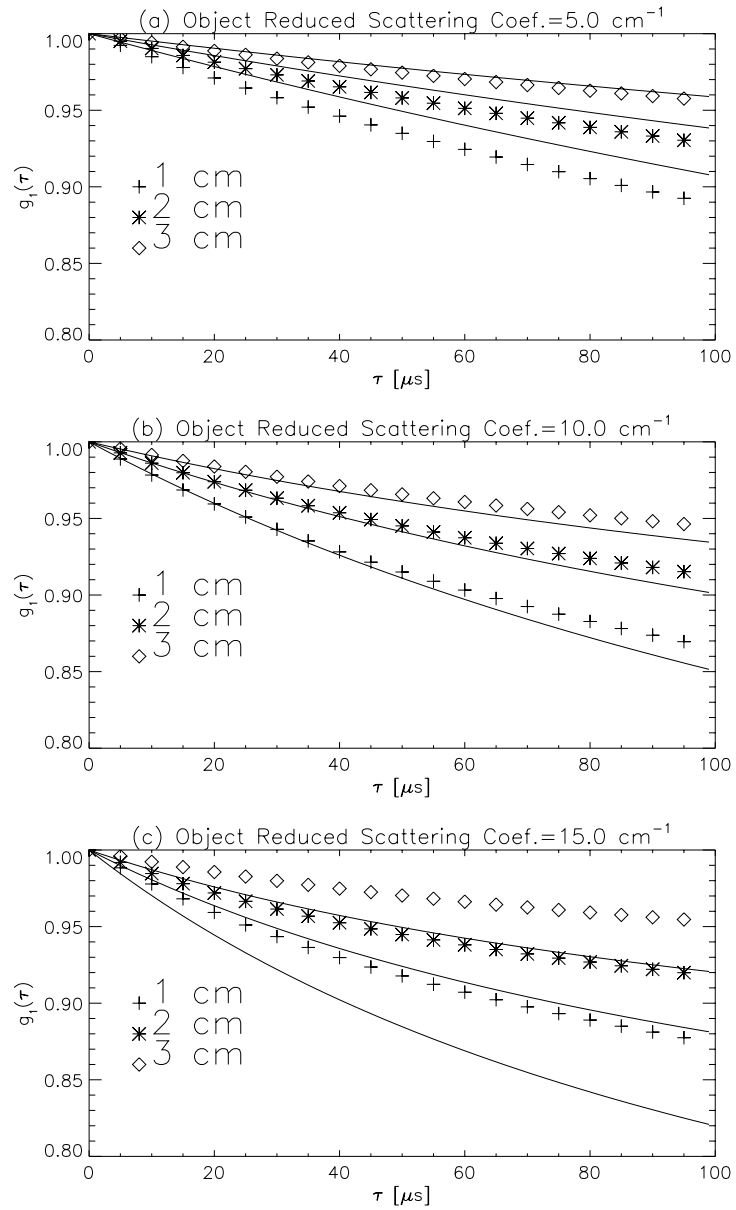
Figure 4.20: Monte Carlo results for $g_1(\tau)$ (symbols) are compared with correlation diffusion theory (lines) for the system depicted in fig. 4.16. In (a), (b), and (c) the object reduced scattering coefficient is respectively 5.0 cm^{-1}, 10.0 cm^{-1}, and 15.0 cm^{-1}. The ρ position of the detector is indicated in the legend. The source is at Sz=2.0 cm and the detector is at Dz=2.0 cm.

4.4.3   Media with Random Flow

Tissue blood flow is a good example of a turbid medium with random flow. Capillary networks are generally randomly oriented on length scales set by the photon random walk step length. When the capillary flow is oriented, as it is in muscle, the photon generally scatters 10+ times between interactions with blood such that the photon's direction is randomized between blood interactions. Thus, the flow is effectively random. Tissue blood flow can be modeled as a two component system, the static tissue matrix and the randomly flowing blood. Monte Carlo results for this system are compared to correlation diffusion theory predictions.

Because the system is composed of two uniformly distributed components, it is necessary to modify the correlation diffusion equation to account for the volume fraction of blood. This is done by simply weighting the dynamical absorption term by the probability of scattering from a red blood cell, i.e.

$$\left(D_\gamma \nabla^2 - v\mu_a - \frac{1}{3} P_{\text{blood}} v\mu_s' k_o^2 \left\langle \Delta V^2 \right\rangle \tau^2 \right) G_1(\mathbf{r}, \tau) = -vS(\mathbf{r}) \ . \qquad (4.52)$$

P_{blood} is the probability of scattering from a red blood cell and is given by

$$P_{\text{blood}} = \frac{\mu_s'(\text{blood})}{\mu_s'(\text{blood}) + \mu_s'(\text{static component})} \ . \qquad (4.53)$$

The other optical parameters in eq. (4.52) account for the combined contribution from the tissue matrix and the blood.

A comparison of the Monte Carlo results and correlation diffusion theory is presented in fig. 4.21 for $P_{\text{blood}} = 0.1$. The optical properties are $\mu_s' = 10.0$ cm^{-1} and $\mu_a = 0.05$ cm^{-1}. The mean square speed of the red blood cells is $\left\langle \Delta V^2 \right\rangle = 1.0$ mm^{2}s^{-2}. The agreement is quite good when $k_o^2 \left\langle \Delta V^2 \right\rangle \tau^2 \ll 1$ indicating that the diffusion theory can be used to quantify blood flow in particular and random flow in turbid media in general. The discrepancy observed for times greater than 25 μs arises from the $k_o^2 \left\langle \Delta V^2 \right\rangle \tau^2 \ll 1$ assumption (note that $[k_o^2 \left\langle \Delta V^2 \right\rangle]^{-1/2} = 61 \ \mu$s). Comparisons were made for other P_{blood} and in all cases good agreement was observed.
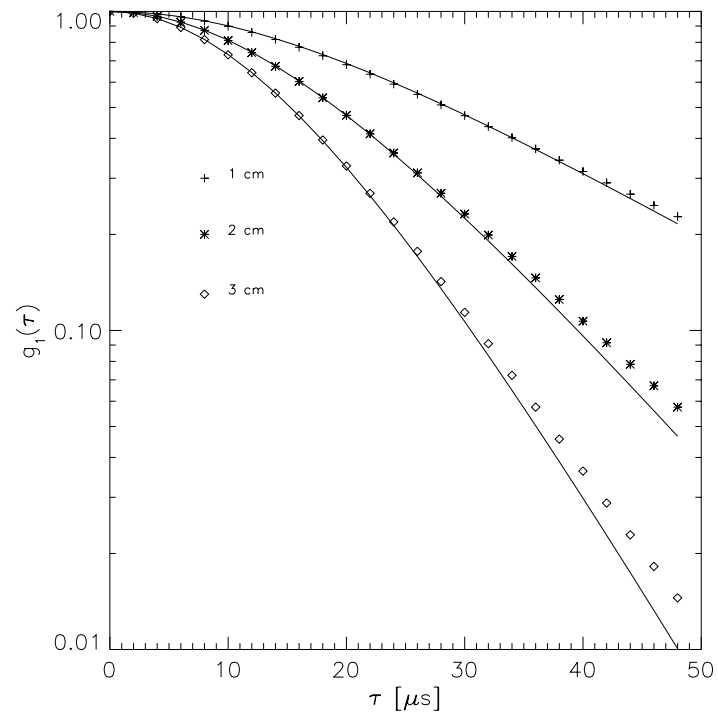
Figure 4.21: Comparison of Monte Carlo simulations and correlation diffusion theory for random flow in a static tissue-like matrix. The probability of scattering from a flow particle (blood) is 0.1.

4.5   Summary

I have shown that the transport of temporal electric field correlation through turbid media can be modeled using a diffusion equation and is thus completely analogous to photon diffusion. The properties of diffusing correlation are thus expected to be similar to the properties of photon diffusion presented in chapter 2. I demonstrated this experimentally by showing that the migration of correlation in a turbid medium with spatially varying dynamical and optical properties can be viewed as a macroscopic scattering of correlation "waves." This concept was shown in the context of both forward and inverse problems. The inverse problem, otherwise known as image reconstruction methods, offers exciting possibilities for studying dynamical variations in heterogeneous turbid media. In biomedical optics, for example, this approach offers a simple framework for analyzing the complex signals obtained from fluid flow in the body. Two different biomedical applications are discussed in the next chapter.